AFRL-SN-RS-TR-2001-125
Final Technical Report
June 2001

SEMICONDUCTOR PHOTONIC COMPONENTS FOR RF APPLICATIONS

University of California

Paul K.L. Yu, A.R. Clawson, G.L. Li, Yuling Zhuang, D.S. Shin, and Phil Mages

APPROVED FOR PUBLIC RELEASE; DISTRIBUTION UNLIMITED.

AIR FORCE RESEARCH LABORATORY
SENSORS DIRECTORATE
ROME RESEARCH SITE
ROME, NEW YORK

This report has been reviewed by the Air Force Research Laboratory, Information Directorate, Public Affairs Office (IFOIPA) and is releasable to the National Technical Information Service (NTIS). At NTIS it will be releasable to the general public, including foreign nations.

AFRL-IF-RS-TR-2001-125 has been reviewed and is approved for publication.

James R. Hunter

APPROVED: JAMES R. HUNTER
Project Engineer

Robert G. Polce

FOR THE DIRECTOR: ROBERT G. POLCE
Chief, Rome Operations Office
Sensors Directorate

If your address has changed or if you wish to be removed from the Air Force Research Laboratory Rome Research Site mailing list, or if the addressee is no longer employed by your organization, please notify AFRL/SNDP, 25 Electronic Pky, Rome, NY 13441-4515. This will assist us in maintaining a current mailing list.

Do not return copies of this report unless contractual obligations or notices on a specific document require that it be returned.

REPORT DOCUMENTATION PAGE			Form Approved OMB No. 0704-0188

1. AGENCY USE ONLY *(Leave blank)*	2. REPORT DATE	3. REPORT TYPE AND DATES COVERED
	Jun 01	Final Jun 99 - Jun 00

4. TITLE AND SUBTITLE
SEMICONDUCTOR PHOTONIC COMPONENTS FOR RF APPLICATIONS

5. FUNDING NUMBERS
C - F30602-99-1-0535
PR - 62204F
PE - 4600
TA - SN
WU - 03

6. AUTHOR(S)
Paul K.L. Yu, A.R. Clawson, G.L. Li, Yuling Zhuang, D.S. Shin, and Phil Mages

7. PERFORMING ORGANIZATION NAME(S) AND ADDRESS(ES)
The Regents of the University of California
University of California, San Diego
Office of Contract & Grant Administration, 0934
9500 Gillman Drive
LaJolla CA 92093-0934

8. PERFORMING ORGANIZATION REPORT NUMBER

9. SPONSORING/MONITORING AGENCY NAME(S) AND ADDRESS(ES)
AFRL/SNDP
25 Electronic Pky
Rome NY 13441-4515

10. SPONSORING/MONITORING AGENCY REPORT NUMBER
AFRL-SN-RS-TR-2001-125

11. SUPPLEMENTARY NOTES
AFRL Project Engineer: James R. Hunter, SNDP, 315-330-7045

12a. DISTRIBUTION AVAILABILITY STATEMENT
Approved for public release; distribution unlimited.

12b. DISTRIBUTION CODE

13. ABSTRACT *(Maximum 200 words)*
The objective of this program was to advance the performance of a semiconductor waveguide modulator in external modulated RF fiber-optic links for space-based and airborne platforms such as true time delay beam formation and beam steering subsystems in phased array antennas. Device and material approaches were investigated to improve the modulator based on semiconductor structures for achieving high spur free dynamic range (SFDR) and high frequency operation. In these approaches, the semiconductor optical modulators were specifically designed to achieve high slope efficiency and high center frequency, while with minimal generation of spurious signals. The fiber-optic links using these modulators are expected to satisfy the low noise figure, high center frequencies, low drive power requirements. The following were the main goals in this program: 1) to design and test electroabsorption waveguide modulator for high multi-octave SFDR and high slope efficiency and high saturation optical power operation, and 2) to collaborate with technical personnel at Air Force Research Laboratory at Rome on the overall link design and provide prototype electroabsorption waveguide modulator for link evaluation.

14. SUBJECT TERMS
Optical Modulator, Optical Waveguide Modulator, Electroabsorption Modulator, RF Photonic Links

15. NUMBER OF PAGES
48

16. PRICE CODE

17. SECURITY CLASSIFICATION OF REPORT	18. SECURITY CLASSIFICATION OF THIS PAGE	19. SECURITY CLASSIFICATION OF ABSTRACT	20. LIMITATION OF ABSTRACT
UNCLASSIFIED	UNCLASSIFIED	UNCLASSIFIED	UL

TABLE OF CONTENTS

LIST OF FIGURES

Technical Objective:

The main objective of this program was to advance the performance of the semiconductor waveguide modulator in the external modulated RF fiber-optic links for space-based and airborne platforms such as true time delay beam formation and beam steering subsystems in phased array antennas. We proposed to investigate device and material approaches to improve the modulator based on semiconductor structures for achieving high spur free dynamic range (SFDR) and high frequency operation. In these approaches, the semiconductor optical modulators would be specifically designed to achieve high slope efficiency and high center frequency, while at the same time maintaining the minimal generation of spurious signals. The fiber-optic links using these modulators are expected to satisfy the low noise figure, high center frequencies, low drive power requirements.

This was a collaborative research program with the University of California at San Diego (UCSD) developing photonic components for fiber links evaluations by the Air Force Research Lab.

The following were the main goals in this program:

1. To design and test electroabsorption waveguide modulator for high multi-octave SFDR and high slope efficiency and high saturation optical power operation.

2. To collaborate with technical personnel at Air Force Research Laboratory at Rome on the overall link design and provide prototype electroabsorption waveguide modulator for link evaluation.

Summary of Accomplishments

1. We have continued the investigation of the critical design and fabrication issues for broadband traveling wave electroabsorption waveguide modulator. A preliminary device has been fabricated.

2. We have continued the investigation of an integrated EA waveguide/mixer for frequency conversion of RF signals that utilizes the electric-field-controlled absorption in an electroabsorption (EA) waveguide. We have compared the performance of the MQW-EA Mixer and FKE-EA Mixer and also evaluated the phase noise properties of the MQW-EA Mixer.

3. We conceived a new approach for linearizing electroabsorption modulators (EAM) for broadband, analog, radio frequency fiber-optic links. In this approach, two or more EAM will be fabricated in series on the same waveguide. Theoretical analysis shows that cancellation of both the second order and third order harmonic distortions can be obtained simultaneously by using proper electrode length and by biasing appropriately the electrodes, leading to an enhancement of the multi-octave spurious free dynamic range (SFDR). Simulation shows that the SFDR of the optical link for the two-electrode case is 10dB larger than that for a single electrode case.

Detailed Technical Achievement On Effort

1. Design and Fabrication of Traveling Wave Electroabsorption Modulator (EAM)

For high-speed application, the bandwidth of the lumped element EAM is known to be RC-time limited. To achieve an ultra large bandwidth in lumped element EAM, the modulation efficiency has to be greatly sacrificed. This is especially critical in analog operation where RF link loss and noise figure must be minimized. To overcome the RC bandwidth limit and to avoid significantly compromising the modulation efficiency, the traveling wave electroabsorption modulator (TW-EAM) has been proposed and experimentally investigated by several authors [1-5].

In our previous work [5], detailed theoretical analysis and numerical calculations have been carried out for ultra high-speed (>50 GHz) TW-EAM, including effects of velocity mismatch, impedance mismatch and microwave attenuation. It was found that due to the optical propagation loss of the waveguide, the TW-EAM waveguide length for maximum RF link gain is limited to 200 ~ 300 μm. A quasi-static equivalent circuit model was used to examine the TW-EAM microwave properties, including the effect of photocurrent. Three TW-EAM design approaches were discussed: low impedance matching; reducing the waveguide capacitance; and distributing the modulation region.

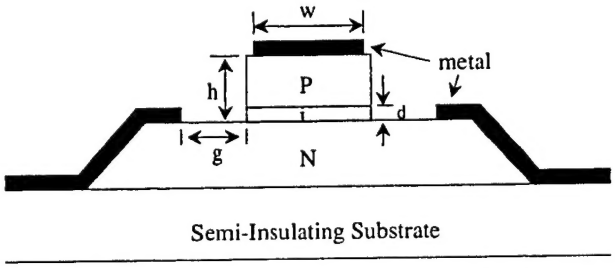

Figure 1. Cross-section of the TW-EAM device.

Continuing from our previous analysis, we have designed and fabricated TW-EAM devices using low impedance matching approach. Figure 1 shows the cross section of the device.

The TW-EAM optical waveguide is similarly designed as that of the lumped element EAMs [6]. Its microwave design is more critical and deserves a more thorough examination.

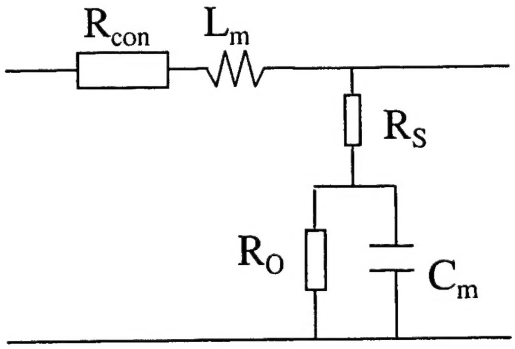

Figure 2. Quasi-static circuit model for a unit length of TW-EAM

The equivalent circuit model we developed, as illustrated in Figure 2, is very helpful in understanding the TW-EAM microwave design. In this circuit model, R_{con} is the conduction resistance, L_m is the inductance, R_s is the device series resistance, C_m is the junction capacitance, R_O is the equivalent ac resistance due to the dependence of the EAM photocurrent on the junction voltage. These circuit parameters determine the TW-EAM frequency response [5]. To achieve ultra large bandwidth, small C_m, R_S and R_{con} are desirable. However, the effect of inductance L_m is not so straightforward to predict. This is illustrated in Figure 3. When the terminator impedance $Z_L > 50\ \Omega$, the waveguide inductance will have little impact on the TW-EAM bandwidth; when $Z_L = 22\ \Omega$, in the L_m range of 0.1 nH/mm to 1.0 nH/mm, a larger L_m will yield a larger bandwidth. This suggests that in our device design which uses a low impedance matching approach, a larger inductance L_m would be preferred.

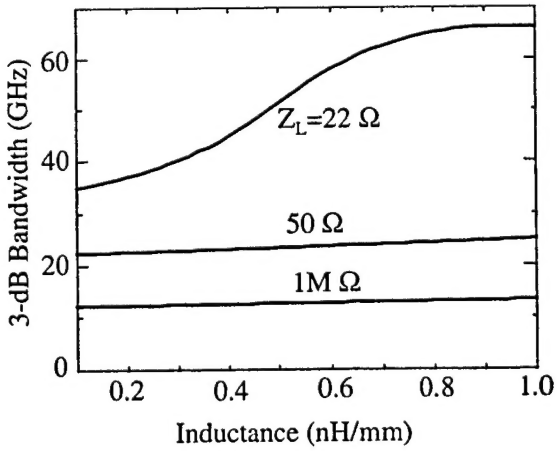

Fig. 3. Effect of waveguide inductance on the 3-dB bandwidth.

The values of all above circuit parameters are determined by the structure design in Figure 1. The capacitance C_m depends upon the waveguide width and the intrinsic layer thickness, which have been determined in the optical waveguide design for maximum modulation efficiency. To achieve a larger inductance, L_m, a smaller central metal width, w, a

larger electrode gap, g, and a larger waveguide height, h, are preferred. However, smaller w causes larger R_{con}; larger g and larger h cause larger R_s. Detailed numerical calculations are needed in order to optimize these structure geometry parameters to obtain the largest bandwidth.

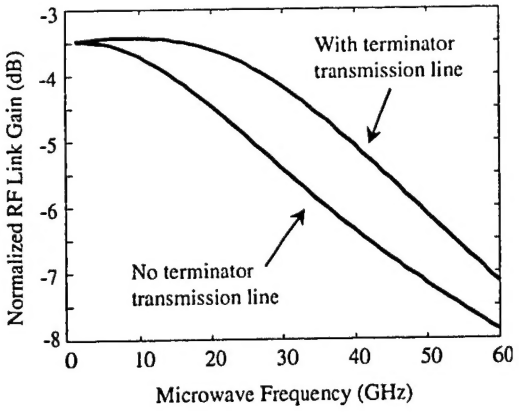

Figure 4. Effect of terminator transmission

In order to connect the low impedance terminator to the TW-EAM waveguide, a microwave transmission line is needed. This transmission line design could have a significant impact to the TW-EAM frequency response. In the calculation we can treat this transmission line plus the terminator as an equivalent terminator. The impedance of this equivalent terminator has an imaginary part that is frequency dependent, which is similar to the TW-EAM waveguide impedance [5]. This infers that a better impedance matching could be achieved by a proper design of the terminator transmission line. However, the transmission line length and impedance have to be optimized in order to get benefit on the TW-EAM bandwidth. More than 10 GHz bandwidth improvement can be obtained with the effect of terminator transmission line, as is illustrated in Figure 4. We have also performed a trade-off analysis of the different device and material parameters.

The device fabrication proceeds in the conventional manner. Previously we used dry etching (RIBE or RIE) that created significant waveguide sidewall roughness. Presently we use wet chemical etching. However, chemical etching usually produces trapezoidal etching profile, which increases the device capacitance. With judiciously chosen etchant and etching conditions, we have successfully obtained a quasi-rectangular waveguide cross-section.

In the lithographic step that connects the metal on top of the waveguide to the bottom electrode on the semi-insulating substrate, extra caution should be exercised, as there are several micrometers difference in height between them. We have presently overcome this difficulty through the use of multiple lithography and specially designed masks.

We have just completed the fabrication of a traveling wave EAM based upon Franz-Keldysh materials. Preliminary evaluation of the transfer curve characteristics shows that the material structure is within the specification of the design. Further microwave evaluation will follow shortly.

2. Performance analysis of the EAM as an optoelectronic mixer for frequency conversion

In a prior work [7], we had proposed and demonstrated an alternate RF signal conversion approach using an electroabsorption (EA) waveguide as a photodetector/mixer. In that approach, frequency converted *electrical* RF signals from the EA waveguide, operating as an optoelectronic mixer (OEM), was generated and made available for subsequent signal processing. The down-converted RF signal can be sent through conventional electrical cable that has low attenuation at baseband/IF frequency. We have demonstrated a moderate conversion loss and high SFDR, RF signal mixing using moderate optical LO power and a simple system configuration [7].

In this program, we compare the performance of the multiple-quantum-well (MQW) and Franz-Keldysh effect (FKE) EA-OEM in this conversion scheme.

In EA waveguides, the electroabsorption process generates an electric-field dependent photocurrent, $I_{ph}(V, P_{opt}) = \eta_m(V) P_{opt}$, where P_{opt} is the optical power and $\eta_m(V)$ is the modulator's detection responsivity. η_m is dependent on the applied bias (therefore, the electric field), and is independent of optical power provided that the device is operated below saturation. When a DC optical power, P_0, and modulation optical power, p at ω_{LO}, are incident on an EA waveguide driven by a DC bias voltage, V_b, along with a RF signal voltage, v at ω_s, the photocurrent generated at the device is given by:

$$I_{ph}(V, P_{opt}) = \eta_m(V_b + v\cos\omega_s t)\cdot(P_0 + p\cos\omega_{LO} t) \qquad (1)$$

The up-and down-converted signals at $\omega_s \pm \omega_{LO}$ are obtained from a small signal analysis of $\eta_m(V_b + v\cos\omega_s t)$ as:

$$I_{ph}^{mix} = \frac{1}{2}\frac{d\eta_m}{dV}\bigg|_{Vb} vp\cos(\omega_s \pm \omega_{LO})t \qquad (2)$$

The higher order derivatives of η_m contribute to the harmonic and intermodulation distortions of this OEM. Note from $d\eta_m/dV|_{Vb}$ in (2) that the electroabsorption is crucial in generating the mixed signals. This distinguishes the electro-absorption mode of the EA-OEM from the usual *pin* photodetection where the responsivity is constant with voltage.

We first compare the current that gives the mixed signals detected by the remote detector, when the EAM is used as a modulator, to the integrated mixer photocurrent. The remote detector photocurrent can be expressed as $I_{trans} = \eta_d P_{opt} t_{ff} T(V)$ where η_d is the responsivity of the remote detector, t_{ff} is the transmission factor of the EAM, and $T(V)$ is the transfer function of the EAM normalized to the incident optical power. The corresponding photocurrent that gives the mixing of ω_s and ω_{LO} is:

$$I_{trans}^{mix} = \frac{1}{2}\eta_d t_{ff}\frac{dT}{dV}\bigg|_{Vb} vp\cos(\omega_s \pm \omega_{LO})t \qquad (3)$$

From I_{ph}^{mix} with I_{trans}^{mix}, the RF power of the converted signals can be obtained, assuming a 50-Ω load resistor. The ratio of powers of the frequency-converted signals in these two cases can be expressed in dB as:

$$Ratio = 20Log\left(\frac{I_{ph}^{mix}}{I_{trans}^{mix}}\right) = 20Log\left(\frac{dI_{ph}/dV}{dI_d/dV}\right) \qquad (4)$$

Here I_{ph} and I_d are the photocurrent detected at the EA-OEM and the remote detector, respectively, and the derivatives are evaluated at the modulator bias, V_b.

In the experiment, AR coated strain-compensated InAsP/GaInP MQW EA waveguide that utilizes the quantum-confined Stark effect [8] and an InGaAsP/InP waveguide [9] that used the Franz-Keldysh effect were compared. The MQW sample has 8 periods of 8.9-nm thick compressively-strained InAsP wells and 7.4-nm thick tensile-strained GaInP barriers, sandwiched by InGaAsP cladding layers. At $\lambda = 1.319$ μm, the transmission (as detected by a remote detector with 0.89-A/W responsivity) and photocurrent characteristics vs. DC bias of the two devices are shown in Fig. 5a and Fig 5b.

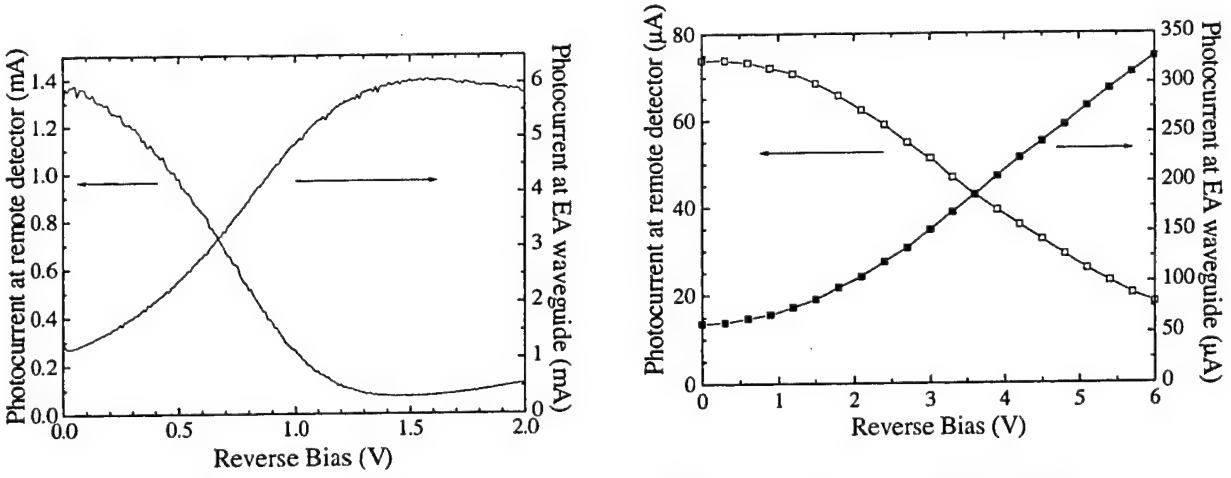

Fig. 5.Transmission and absorption characteristics of (a) the MQW (at 10 mW), (b) bulk InGaAsP waveguides (at 1 mW).

The normalized slope efficiencies are -1.1 V^{-1} and -0.18 V^{-1}, respectively, for these transmission curves. The fiber-to-fiber insertion loss of the waveguides are 8.0 dB and 11 dB, respectively.

The RF-frequency-mixing setup is shown in Fig. 6 with two Nd:YAG lasers generating a beat tone at a 100-% modulation depth, which was used as an optical LO signal to the EA waveguide. Electrical voltage that contained the DC bias as well as the RF signal at ω_s was applied to the EA-OEM under test.

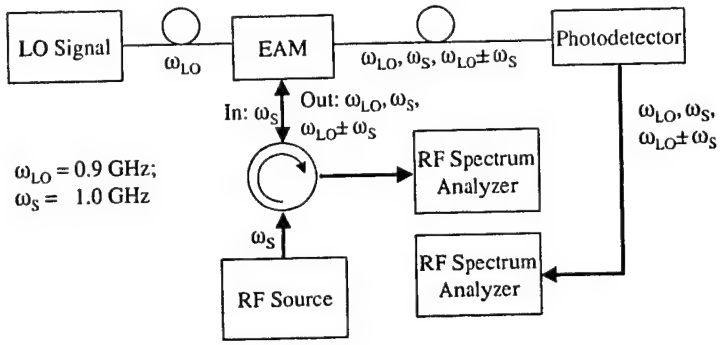

Fig. 6. Experimental set-up for the mixing experiment using the EA waveguide.

The DC bias was first set at the second order null point of the transmission curve, which corresponds to the highest slope efficiency of the photocurrent vs. DC bias curve. When the RF signal power was increased from –20 dBm to –10 dBm, the converted signal powers increased by 10 dB. They closely follow the behavior predicted by (2). The MQW EA waveguide became saturated around 10-mW of LO optical power.

Defining the conversion loss as the ratio of the input RF signal power to the output frequency converted signal power, the conversion loss for the case when the MQW EA-OEM was used as a photodetector/mixer is measured at 18.9 dB. This conversion loss is mainly limited by LO optical power (10 mW) and the saturation power of the MQW waveguide. When this MQW EA waveguide was used as a modulator/mixer and the converted signals were transmitted through the optical fiber, the conversion loss was increased to 27.8 dB. The increase in conversion loss is mainly due to the fact that the responsivity of the remote detector, η_d at the end of the fiber link combined with the EA waveguide insertion loss, t_{ff}, was much smaller than that of the EA waveguide.

Two-tone SFDR measurement was carried out with the RF tones at 1.00 and 1.02 GHz and the optical LO tone at 0.90 GHz. The converted signals and the their third-order intermodulation distortions (IMD_3's) were measured. (Due to the bandwidth limitation of the circulator, only the up-converted signals were measured.) When the MQW EA waveguide was biased at the highest slope point of the device photocurrent vs. DC bias curve (second-order null point), a SFDR of 102.4 dB-$Hz^{2/3}$ was obtained at 10-mW optical LO power for the up-converted signal at 1.90 GHz. When the MQW EA-OEM was biased at the third-order null point of the device photocurrent vs. DC bias curve, the up-converted RF signal power was reduced by ~3 dB, but the sub-octave SFDR was measured at 120.0 dB-$Hz^{4/5}$ with the fifth-order dependence on the input RF power. At the third-order null point, the IMD_3 due to the third-order input power dependence becomes null, making the IMD_3 depending on the next order, which is the fifth order.

For the InGaAsP FKE EA-OEM, a larger RF conversion loss (29.2 dB) was measured at the same LO optical power of 10 mW, mainly due to the smaller slope efficiency of the FKE. However, the single-octave SFDR's of this photodetector/mixer are within 4 dB of those of the above MQW device, primarily due to the lower degree of saturation of the FKE device at 10 mW. These results are summarized in Table 1.

Device	Conversion loss (dB)	SFDR
InAsP/GaInP MQW	18.9 (2^{nd} order null) 21.9 (3^{rd} order null)	102 dB-$Hz^{2/3}$ 120 dB-$Hz^{4/5}$
Bulk InGaAsP	29.2 (2^{nd} order null) 33.2 (3^{rd} order null)	98 dB-$Hz^{2/3}$ 117 dB-$Hz^{4/5}$

Table 1. EA-OEMs at 10 mW optical LO power.

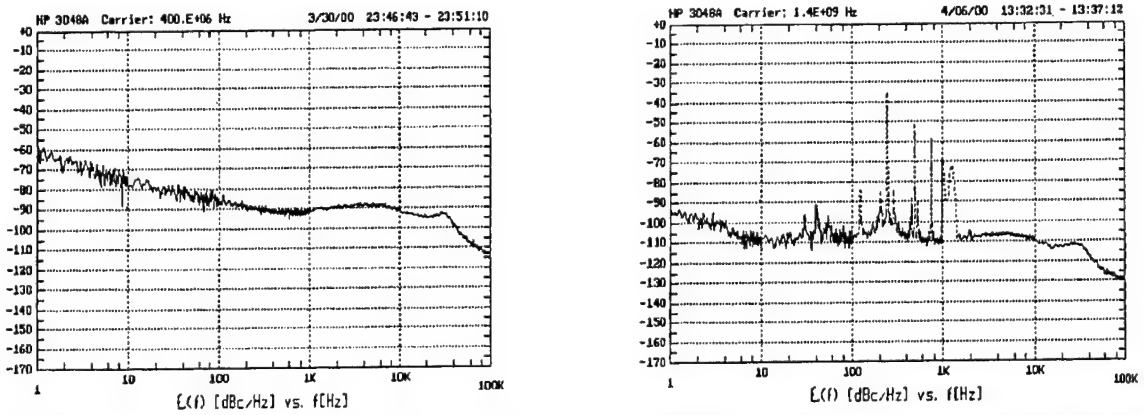

Fig. 7a. Absolute phase noise of the RF source driving the MZM (optical LO generator). b. Residual phase noise characteristic of the EA-OEM up-converted signal at 1.4 GHz

We have also measured the phase noise characteristics of the converted signals. In the measurement, the optical LO (Fig. 7a) is generated via external modulation of a high power laser using a lithium niobate MZM. Fig. 7b shows the residual phase noise spectrum of the up-converted using a 400 MHz optical LO signal.

In this program, we have demonstrated that the EA waveguide can be utilized as an OEM that possesses low phase noise, large SFDR conversion properties. The conversion loss and SFDR are both dependent on the slope efficiency and saturation power level. At 10-mW LO power, a sub-octave SFDR of 120.0 dB-$Hz^{4/5}$ was achieved with the MQW EA-OEM.

3. Analysis of the Multi-Electrode Linearized EA modulator

In this project, we conceived a new linearized design of EAM by using two or more electrodes fabricated in tandem. Fig. 8 shows the two-electrode case. Different biases are applied on the two electrodes. By properly choosing the biases and the electrode lengths, certain orders of non-linearity can cancel each other. Thus the SFDR of the RF optical fiber link can be increased. Theoretical analysis and simulation results of two electrodes in tandem carried out. The linearization technique involved here can also apply to two dissimilar modulators in tandem. Experimentally, we have demonstrated the distortion cancellation effect using one EA modulator and one Mach-Zehnder in series. Cancellation of harmonics is obtained by changing the biases of these two modulators.

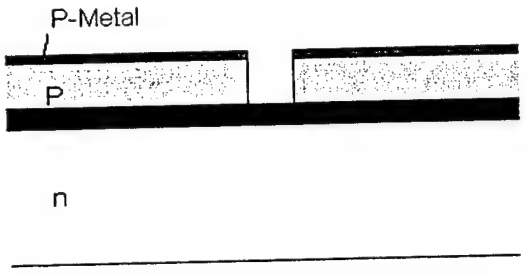

Fig. 8. Structure of two-electrode Modulator.

The transmission function of the one-electrode EA modulator is modeled as:

$$T = e^{-\Gamma \alpha L} \qquad (5)$$

Here, Γ is the optical confinement factor of the absorption layer, α is the optical absorption coefficient of the absorption layer, L is the optical waveguide length. And $\alpha = \alpha_b + \Delta\alpha$, where α_b is absorption coefficient at DC bias V_b, $\Delta\alpha$ is the change of α in the material due to the RF voltage V_{RF}..

In the two-electrode scheme, we break the electrode L into two sections. It is equivalent to two electroabsorption modulators under different DC bias connected in series. The same V_{RF} is applied to both electrodes. The total transmission function is the product of the two transmission functions.

$$T = e^{-\Gamma \alpha_1 L_1} \cdot e^{-\Gamma \alpha_2 L_2} \qquad (6)$$

Here, $\alpha_1 = \alpha_{b1} + \Delta\alpha_1$, α_{b1} is the absorption coefficient at DC bias V_{b1}, $\alpha_2 = \alpha_{b2} + \Delta\alpha_2$, α_{b2} is the absorption coefficient at DC bias V_{b2}, L_1 is the length of the first electrode biased at V_{b1}, L_2 is the length of the second electrode biased at V_{b2}, $L = L_1 + L_2$.

Taylor expanding Eq. (5) at the DC bias points V_{b1} and V_{b2}, we get

$$T = T|_{V_{RF}=0} + \sum_k (V_{RF} \sin \omega t)^k \cdot h_k \qquad (7)$$

where, $h_k = \frac{1}{k!}\left(\frac{\partial^k T}{\partial V^k}\right)\Big|_{V=V_{b1},V_{b2}}$ is the coefficient of the $\sin \omega t$ to the k^{th} power.

From equation (6), we obtain the following results when $h_2 = 0$.

$$L_1 \frac{\partial^2 \alpha_1}{\partial V^2}\Big|_{Vb1} + L_2 \frac{\partial^2 \alpha_2}{\partial V^2}\Big|_{Vb2} = \Gamma (L_1 \frac{\partial \alpha_1}{\partial V}\Big|_{Vb1} + L_2 \frac{\partial \alpha_2}{\partial V}\Big|_{Vb2})^2$$

and

$$\begin{cases} L_1 \frac{\partial^2 \alpha_1}{\partial V^2}\Big|_{Vb1} + L_2 \frac{\partial^2 \alpha_2}{\partial V^2}\Big|_{Vb2} = \Gamma (L_1 \frac{\partial \alpha_1}{\partial V}\Big|_{Vb1} + L_2 \frac{\partial \alpha_2}{\partial V}\Big|_{Vb2})^2 \\ L_1 \frac{\partial^3 \alpha_1}{\partial V^3}\Big|_{Vb1} + L_2 \frac{\partial^3 \alpha_2}{\partial V^3}\Big|_{Vb2} = 2\Gamma^2 (L_1 \frac{\partial \alpha_1}{\partial V}\Big|_{Vb1} + L_2 \frac{\partial \alpha_2}{\partial V}\Big|_{Vb2})^3 \end{cases}$$

when $h_2=0$ and $h_3=0$.

In order to illustrate the analysis given above, we consider first the simplest case $L_1=L_2=L/2$. We show that the simulated SFDR of the link with a two-electrode modulator is significantly larger than that of the one-electrode case. $(\sin\omega t)^4$ and $(\sin\omega t)^5$ contributions to the fundamental, 2nd harmonic and 3rd harmonic are included. Other higher order contributions are neglected. For modulator using Franz-Keldysh effect, we obtained a 10 dB improvement of the multi-octave SFDR, as summarized in Table 2

	DC bias	**SFDR**	h_1
Two-electrode	V_{b1}=1.412V V_{b2}=0.910V	104.2dBc	-0.33
One-Electrode	V_b=1.161V (2nd order null point)	95.0dBc	-0.34

Table 2

Using published data for the MQW transfer curve [7], we obtained similar improvement, as shown in Table 3.

	DC bias	**SFDR**	h_1
Two-electrode	V_{b1}=0.82V V_{b2}=0.49V	102.4dBc	-1.11
One-Electrode	V_b=0.72V (2nd order null point)	93.3dBc	-1.17

Table 3

Similar simulations have been performed for two-electrode modulators with unequal lengths ($L_1 \neq L_2$). We can improve the SFDR even more by adjusting L_1 and L_2. However, the increase in h_4 and h_5 will limit the SFDR improvement. Comparing with the results obtained for the equal length case, the difference is minor, just about 3~4 dBc.

We have done preliminary experimental analysis, the data collected from MZM and EAM in tandem show a decrease of 12dB in 3rd order harmonic with almost no change in 2nd harmonic and only 1.5dB penalty in reduction of fundamental signal.

References:

1. K. Kawano, M. Kohtoku, M. Ueki, T. Ito, S. Kondoh, Y. Noguchi and Y. Hasumi, *Electron. Lett.*, vol. 33, pp. 1580-1581, 1997.
2. H. H. Liao, X. B. Mei, K. K. Loi, C. W. Tu, P. M. Asbeck and W. S. C. Chang, *Proc. SPIE, Optoelectronic Integrated Circuits,* vol. 3006, pp. 291-300, 1997.
3. S. Z. Zhang, Y. J. Chiu, P. Abraham and J. E. Bowers, *IEEE Photon. Technol. Lett.*, vol. 11, pp.191-193, 1999.
4. W. S. Cho, Y. S. Lim and Y. W. Choi, *MWP'99 digest,* pp. 153-156, 1999.
5. G. L. Li, C. K. Sun, S. A. Pappert, W. X. Chen and P. K. L. Yu, *IEEE Trans. on Microwave Theory and Techniques*, vol. 47, pp. 1177-1183.1999.
6. G. L. Li, R. B. Welstand, W. X. Chen, J. T. Zhu, S. A. Pappert, C. K. Sun, Y. Z. Liu and P. K. L. Yu, *IEEE Photonics Technol. Letts.*, vol.10, pp.672-674, 1998.
7. D. S. Shin, G. L.Li, C. K. Sun, K. K. Loi, W. S. C. Chang, P. K. L. Yu, IEEE Photon. Technol. Lett., **12**, pp. 193-195, 2000.
8. K. K. Loi, J. H. Hodiak, W. B. Mei, C. W. Tu, W. S. C. Chang, D. T. Nichols, L. J. Lembo, and J. C. Brock, *IEEE Photon. Technol. Lett.*, **10**, pp. 1572-1574, 1998.
9. G. L. Li, Y. Z. Liu, R. B. Welstand, C. K. Sun, W. X. Chen, J. T. Zhu, S. A. Pappert, and P. K. L. Yu, *IEEE Photon. Technol. Lett.*, vol. 11, pp.659-61, 1999.

Publications supported by this contract

1. D. S. Shin, G. L. Li, W. S. C. Chang, P. K. L. Yu, C. K. Sun, S. A. Pappert, and Y. Z. Liu, "Electroabsorption Waveguide as an Integrated Photodetector/Mixer for RF Frequency Conversion", Proceedings of the Tenth Annual DARPA Symposium on Photonic Systems for Antenna Applications, Session 7, 8 pages (2000).
2. Y. Zhuang, G. L. Li, W. S. C. Chang, P. K. L. Yu, and Y. Z. Liu, " Analysis of the Multi-Electrode Linearized EA modulator" Proceeding of SPIE, 4112, paper 02, 2000.

3. G. L. Li, D. S. Shin, W. S. C. Chang, P. M. Asbeck, P. K. L. Yu, C. K. Sun, S. A. Pappert, and R. Nguyen, "Design and Fabrication of Traveling Wave Electroabsorption Modulator", Proceeding SPIE 3950, paper 33, 2000
4. D. S. Shin, G. L. Li, C. K. Sun, S. A. Pappert, W. S. C. Chang, and P. K. L. Yu, " Performance of the Electroabsorption Modulator as an Integrated Optoelectronic Mixer for RF Frequency Conversion", IEEE International Meeting on Microwave Photonics, Oxford, England, Sept. 2000 Paper Tu. 2.5, pp. 70-73, 2000

Acknowledgments

The work reported here is mainly supported by the AFRL program. Additional fundings are obtained from AASERT program, the California MICRO program, Raytheon, and ONR.

APPENDIX - Publications

1. Electroabsorption Waveguide as an Integrated Photodetector/Mixer for RF Frequency Conversion
2. Analysis of the Multi-electrode Linearized EA Modulator
3. Design and Fabrication of Traveling Wave Electroabsorption Modulator
4. Performance of the Electrobsorption Modulator as an Integrated Optoelectronic Mixer for RF Frequency Conversion

Submitted to PSAA-10
Monterey, 2000

Electroabsorption Waveguide as an Integrated Photodetector/Mixer For RF Frequency Conversion

D. S. Shin, G. L. Li, W. S. C. Chang, and P. K. L. Yu
Dept. of Electrical and Computer Engineering
University of California, San Diego, La Jolla, CA 92093-0407
Telephone: 858 534 6570; Fax: 858 534 0556; E-mail: dshin@ucsd.edu

C. K. Sun and S. A. Pappert,
SPAWAR Systems Ctr.; San Diego, CA 92152-5001
Telephone: 619 553 1160; Fax: 619 553 1060, E-mail: cksun@nosc.mil

Y. Z. Liu
Fermionics Lasertech
1153 Lawrence Drive, Newbury Park, CA 91320
Telephone: 805 373 0999; Fax: 805 375 0339; E-mail: yzliu@pacbell.net

Abstract: An integrated photodetector/mixer for frequency conversion of RF signals is demonstrated utilizing the electric-field-controlled absorption in an electroabsorption (EA) waveguide. Applying this approach to an InAsP/GaInP multiple-quantum-well EA waveguide, a conversion loss of 18.4 dB was obtained at 10-mW optical local oscillator power, and a sub-octave, two-tone spur-free dynamic range of 120.0 dB-$Hz^{4/5}$ was measured for an up-converted signal at 1.9 GHz.

Summary: Microwave photonics is considered to be a viable alternative technology in application areas where electronics has traditionally played a central role. Frequency converting photonic links for antenna remoting applications is a good example of this where antenna front-end hardware complexity may be minimized and the deleterious effects of fiber dispersion may be avoided [1,2]. Many of the conversion schemes take advantage of the optical local oscillator (LO), which is less complex than the electronic LO at high frequency, and has shown lower phase noise [3]. There have been several proposals to achieve low conversion loss and large spur-free dynamic range (SFDR) for photonic frequency converting links [4-6]. One approach makes use of Mach-Zehnder modulators at very high optical LO power (350 mW) to achieve positive link conversion gain (defined as the ratio of the output converted RF power to the input RF power) [5,6]. An alternative approach uses either a heterojunction phototransistor or heterojunction bipolar transistor (HBT) to convert the modulated optical radiation to the RF signal, by using the inherent nonlinearity of the device [7-9]. In [8], a 10.4-dB intrinsic conversion gain (-5.5 dB external conversion gain) was achieved using an electrical LO. In [9], two HBT's in a cascode configuration were used to achieve an intrinsic conversion gain of 18.2 dB and an extrinsic conversion gain of 7.4 dB with a three-stub tuner.

In this work, a new RF signal conversion approach is proposed and demonstrated using an electroabsorption (EA) waveguide as a photodetector/mixer. Unlike previous

approaches [1,2,4-6], frequency converted electrical RF signals from the EA waveguide, operating as an optoelectronic mixer (OEM), are generated and made available for subsequent signal processing. This converted RF signal can be sent through conventional electrical cable that has low attenuation at baseband/IF frequency. This avoids using high LO power to compensate the fiber RF link loss. We have demonstrated a moderate conversion loss and high SFDR RF signal mixing using moderate optical LO power and a simple system configuration.

When optical power is incident on EA waveguides, the electroabsorption process generates an electric-field-dependent photocurrent, I_{ph}, expressed as $I_{ph}(V, P_{opt}) = \eta_m(V) P_{opt}$, where P_{opt} is the optical power and $\eta_m(V)$ is the modulator's detection responsivity. As depicted in Fig. 1, η_m is dependent on the applied bias (therefore, the electric field), and is independent of optical power provided that the device is operated below saturation. When a DC optical power, P_0, and modulated optical power, p at ω_{LO}, are incident on an EA waveguide driven by a DC bias voltage, V_b, along with a RF signal voltage, v at ω_s, the device photocurrent is given by:

$$I_{ph}(V, P_{opt}) = \eta_m(V_b + v\cos\omega_s t)\cdot\left(P_0 + p\cos\omega_{LO} t\right). \qquad (1)$$

Using a small signal analysis of $\eta_m(V_b + v\cos\omega_s t)$, the up-and down-converted signals at $\omega_s \pm \omega_{LO}$ are obtained as:

$$I_{ph}^{mix} = \frac{1}{2}\frac{d\eta_m}{dV}\bigg|_{Vb} vp\cos(\omega_s \pm \omega_{LO})t, \qquad (2)$$

where $\left.\frac{d\eta_m}{dV}\right|_{Vb}$ is the first-order derivative evaluated at the DC bias voltage. The higher order derivatives of η_m will contribute to the harmonic and intermodulation distortions of this OEM. Note from $\left.\frac{d\eta_m}{dV}\right|_{Vb}$ in (2) that the electro-absorption is crucial in generating mixed signals. This distinguishes the EA waveguides in the detector mode [10] from the usual *pin* photodetector that is biased to give a constant responsivity with voltage.

In this work, we compare the current that gives the mixed signals detected by the remote detector, when the EAM is used as a modulator. The current detected by the remote detector can be expressed as $I_{trans} = \eta_d P_{opt} t_{ff} T(V)$, where η_d is the responsivity of the remote detector, t_{ff} is the transmission factor of the EAM, and $T(V)$ is the transfer function of the EAM normalized to the incident optical power. The corresponding photocurrent that gives the mixing of ω_s and ω_{LO} is:

$$I_{trans}^{mix} = \frac{1}{2}\eta_d t_{ff}\frac{dT}{dV}\bigg|_{Vb} vp\cos(\omega_s \pm \omega_{LO})t. \qquad (3)$$

From I_{ph}^{mix} with I_{trans}^{mix}, the RF power of the converted signals can be calculated, assuming 50-Ω load resistor dissipating the RF power. The ratio of powers of the frequency conversion signals in these two cases can be calculated in dB as:

$$Ratio = 20Log\left(\frac{I_{ph}^{mix}}{I_{trans}^{mix}}\right), \qquad (4)$$

which can be expressed with DC transfer curve parameters as follows:

$$Ratio = 20Log\left(\frac{dI_{ph}/dV}{dI_d/dV}\right). \quad (5)$$

Here I_{ph} and I_d are the DC photocurrent detected at the EAM and remote detector, respectively, and the derivatives are evaluated at the operating bias, V_b.

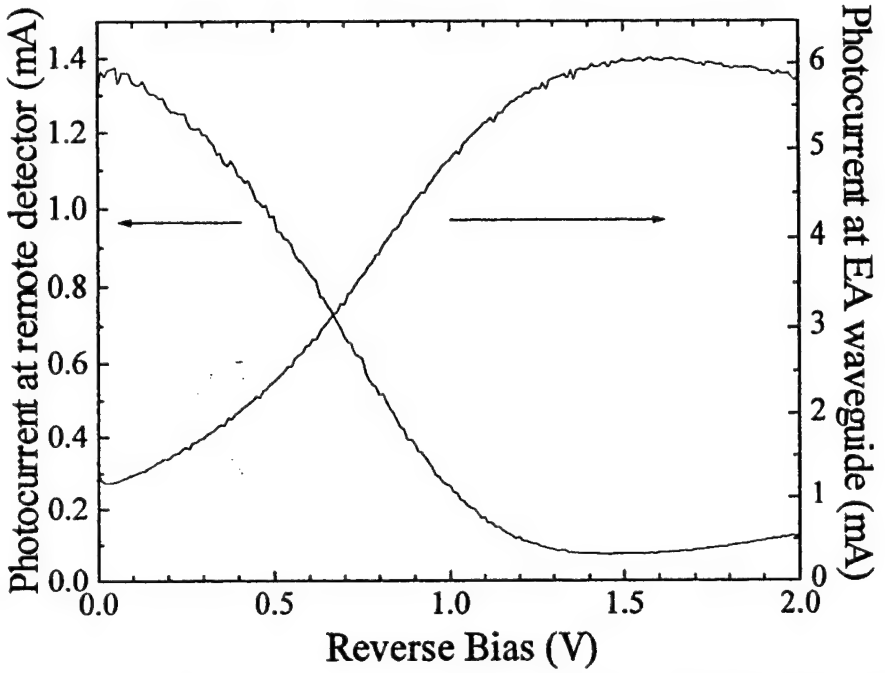

Fig. 1. Transmission (photocurrent at remote detector) and absorption (photocurrent at modulator) characteristics of the MQW EA waveguide used. Optical power of 10 mW at 1.319 μm is used.

In the experiments, an anti-reflection coated strain-compensated InAsP/GaInP multiple-quantum-well (MQW) EA waveguide that utilizes the quantum-confined Stark effect (QCSE) was used [11]. The undoped electroabsorption layer was composed of 8 periods of 8.9-nm thick compressively-strained InAsP wells and 7.4-nm thick tensile-strained GaInP barriers, sandwiched by InGaAsP cladding layers. At an optical power of 10 mW (λ = 1.319 μm), the transmission (as detected by a remote detector with 0.89-A/W responsivity) and device photocurrent characteristics vs. DC bias of this EA waveguide are shown in Fig. 1. The normalized slope efficiency is -1.1 V^{-1} for the transmission curve. The fiber-to-fiber insertion loss of this waveguide as a modulator was estimated to be 8.0 dB. The electrical 3-dB bandwidth of this device was separately measured to be 4.8 GHz without using a 50-Ω matching resistor. The length of this waveguide device was 185 μm.

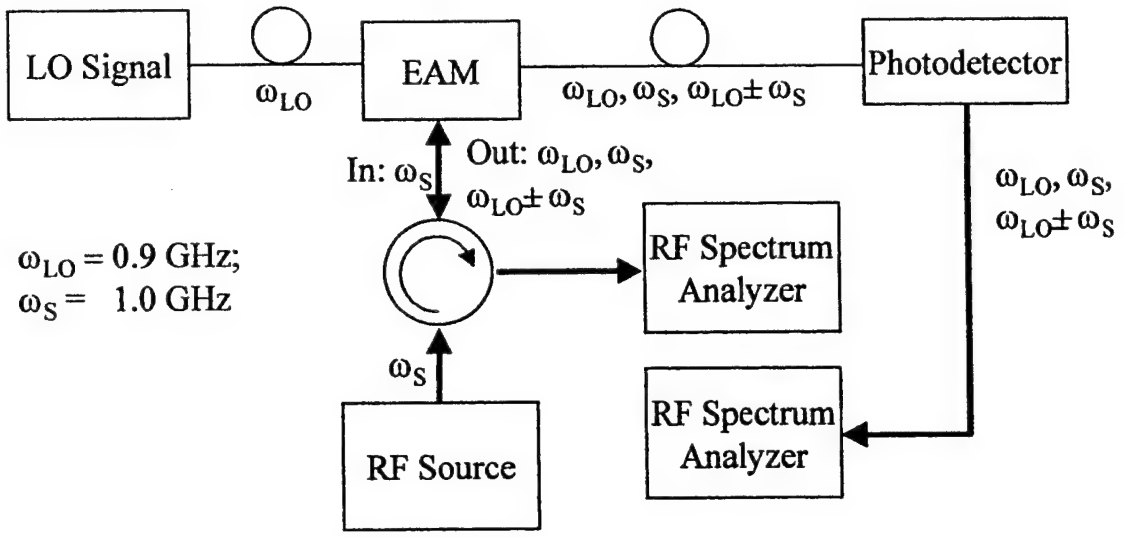

Fig. 2. Experimental set-up for the mixing experiment using the EA waveguide.

The RF frequency mixing experiment was set up as shown in Fig. 2. Two Nd:YAG lasers were set up to generate a beat tone at 900 MHz with 100-% modulation depth, which was used as an optical LO signal to the EA waveguide OEM. Electrical voltage that contained the DC bias as well as the RF signal at ω_s = 1.0 GHz was applied to the device. The DC bias used was –0.75 V, which corresponds to the highest slope efficiency of the photocurrent vs. DC bias curve. A RF circulator (bandwidth 1~2 GHz) was inserted between the device under test and the RF spectrum analyzer to measure the RF power generated at the device.

Fig. 3 (a) summarizes the measured RF signals from the EA waveguide. The optical LO power incident on the EA waveguide was 10 mW, and the input RF power was –20 dBm. The LO was observed at 900 MHz, and the signal at 1.0 GHz. Up-converted signal power detected at 1.9 GHz was –38.9 dBm after calibration of the microwave loss due to the cables. In Fig. 3, other RF signals are also evident, e.g., second harmonics of the LO at 1.8 GHz; down-converted signal at 0.1 GHz; third-order intermodulation distortions (IMD_3) of the LO and the RF signal at 0.8 GHz, etc. The up- and down-converted signals appear to have different RF power, caused by the bandwidth limitation of the circulator. When the RF signal power was increased to –10 dBm, the converted signal powers increased by 10 dB. They closely follow the behavior predicted by (2). It was also found that the device became saturated around 10-mW LO optical power. Compared with the measurement at low optical power (1 mW), the RF link gain comprised of this EA waveguide as an external modulator was compressed by 4 dB at 10 mW.

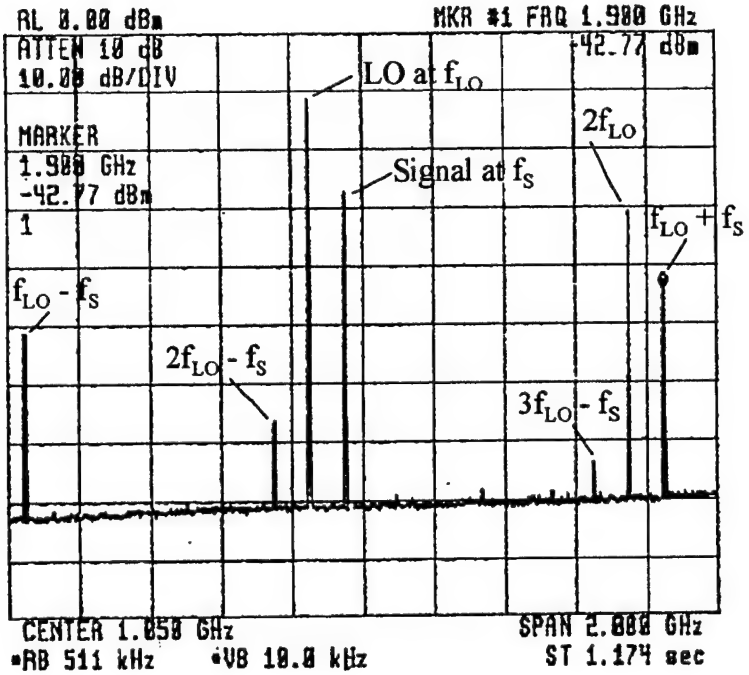

(a)

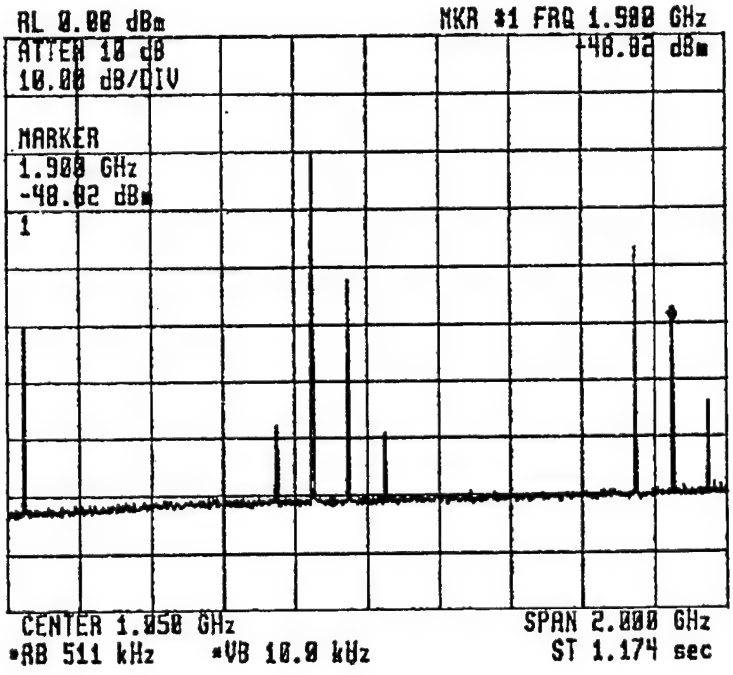

(b)

Fig. 3. Measured RF spectrum (a) at the EA waveguide, (b) at the remote detector.

Fig. 3 (b) shows the RF power transmitted through the fiber and detected by the remote detector. It has a similar RF spectrum as Fig. 3 (a), but due to the link loss, the original signal power at ω_s is attenuated (link loss = 21 dB). Up-converted signals are now measured to be –48.8 dBm. (After microwave-loss calibration, the power becomes –47.8 dBm.) Up- and down-converted signals are observed to have the same power. When we measure the mixing using an increased signal power –10 dBm from –20 dBm, the converted signal powers increase by 10 dB, which closely follows the behavior predicted by (3).

Defining the conversion loss as the ratio of the input RF signal power to the output converted signal power, the conversion loss for the case when the EA waveguide was used as a photodetector/mixer is found to be 18.9 dB. The conversion loss obtained above is mainly limited by LO optical power and the saturation power of the EA waveguide used. It could be improved by using an EA waveguide with higher saturation. Increasing the LO power can increase the converted RF power, as shown in (2). Decreasing the coupling loss from the fiber to the EA waveguide is another approach, which also increases η_m. When this EA waveguide was used as a modulator/mixer and the converted signals were transmitted through the optical fiber as in [4-6], the conversion loss was increased to 27.8 dB. The increase in conversion loss (8.9 dB) is mainly due to the fact that the responsivity of the remote detector, η_d at the end of the fiber link combined with the EA waveguide insertion loss, t_{ff}, was much smaller than that of the EA waveguide, η_m, i.e., $t_{ff}\eta_d < \eta_m$.

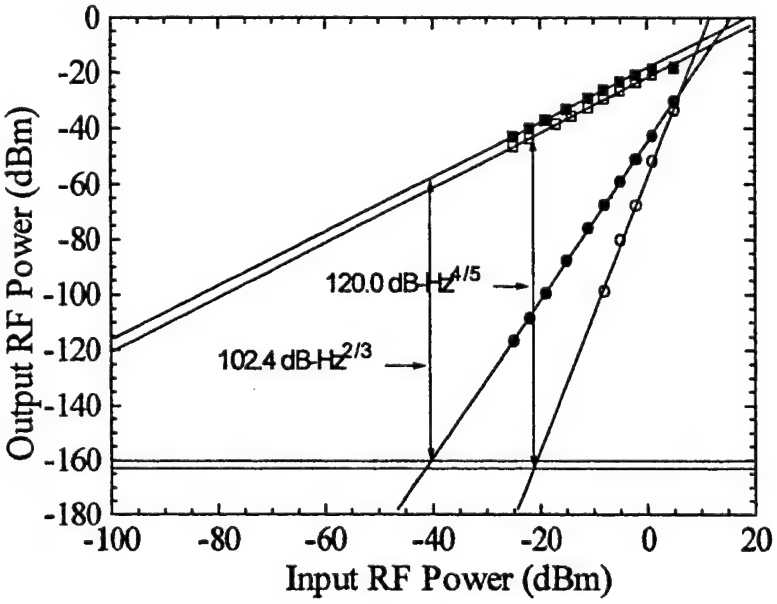

Fig. 4. Two-tone test of the MQW EA photodetector/RF mixer. Converted RF signals (■: for highest slope point, □: for third-order null point) and the IMD_3's (●: for highest slope point, ○: third-order null point) are shown. Noise floors (dotted lines) were

dominated by the shot noise and given by –160 dBm/Hz and –163 dBm/Hz for the highest slope point and the third-order null point, respectively

The two-tone SFDR of the EA waveguide photodetector/RF mixer was also measured, as shown in Fig. 4. With two RF tones at 1.00 and 1.02 GHz and the optical LO tone at 0.90 GHz, the converted signals and the their IMD_3's were measured. (Due to the bandwidth limitation of the circulator, only the up-converted signals were measured.) When the EA waveguide was biased at the highest slope point of the device photocurrent vs. DC bias curve (second-order null point), a SFDR of 102.4 dB-$Hz^{2/3}$ was obtained at 10-mW optical LO power for the up-converted signal at 1.90 GHz. The noise floor was dominated by the shot noise due to the device photocurrent. When the EA waveguide was biased at the third-order null point of the device photocurrent vs. DC bias curve (0.44 V), the up-converted RF signal power was reduced by ~3 dB, but the suboctave SFDR was measured at 120.0 dB-$Hz^{4/5}$ with the fifth-order dependence on the input RF power. At the third-order null point, the IMD_3 due to the third-order input power dependence becomes null, making the IMD_3 depending on the next order, which is the fifth order [4,12]. To the authors' knowledge, this result is among the best SFDR ever reported in the semiconductor-based approach, and compares favorably with the best SFDR in the other approach [6], considering the optical LO power used.

A bulk InGaAsP-InP EA waveguide [13] that uses the Franz-Keldysh effect was also tested for RF signal conversion. The transmission characteristic of the Franz-Keldysh EA device is shown in Fig. 5. Larger RF conversion loss (29.2 dB) was measured when this EA waveguide was used as a photodetector/mixer at the same LO optical power of 10 mW, than those obtained with MQW waveguides. This result is mainly due to the smaller slope efficiency (0.18 V^{-1}) of the bulk EA waveguide and demonstrates the importance of the slope efficiency of the EA waveguide when it is utilized as a photodetector/mixer.

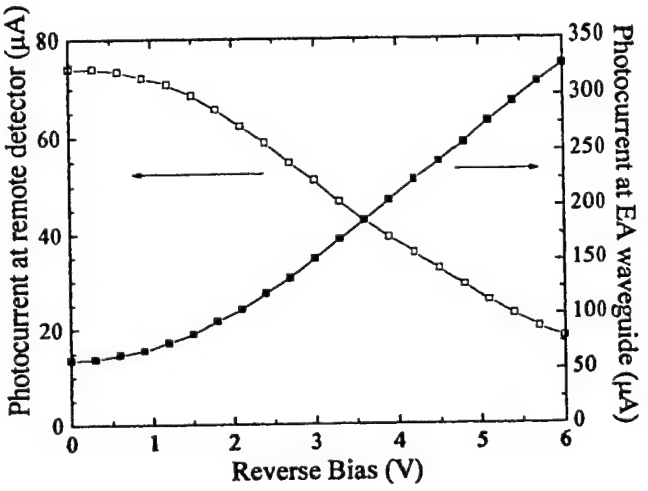

Fig. 5. Transmission (photocurrent at remote detector) and absorption (photocurrent at modulator) characteristics of the Franz-Keldysh EA waveguide for an optical power of 1 mW at 1.319 μm. Fiber-to-fiber insertion loss was 10.7 dB.

In conclusion, we have demonstrated that the MQW EA waveguide can be utilized as an OEM that combines both functions of a photodetector and an electronic mixer. Conversion loss and dynamic range have been measured for this OEM device. At 10-mW LO power, a sub-octave SFDR of 120.0 dB-$Hz^{4/5}$ was measured. It has been pointed out that the slope efficiency of the EA waveguide is extremely important in determining conversion gain. Currently 18.9 dB conversion loss has been obtained and this result can be reduced with higher optical power. This scheme can be useful in antenna applications where optical LO signal distribution is used for frequency converting microwave signals.

Acknowledgement

This work is partially supported by DARPA/AFRL, ONR and MICRO-Raytheon. The authors like to acknowledge Dr. K. K. Loi for providing the MQW samples.

References

1. G. K. Gopalakrishnan, R. P. Moeller, M. M. Howerton, W. K. Burns, K. J. Williams, and R. D. Esman, *IEEE Trans. Microwave Theory Tech.*, vol. 43, pp. 2318-2323, 1995.
2. K.-I. Kitayama, and R. A. Griffin, *IEEE Photon. Technol. Lett.*, vol. 11, pp. 287-289, 1999.
3. X. S. Yao, and L. Maleki, *IEEE J. Quantum Electron.*, vol. 32, pp. 1141-1149, 1996.
4. C. K. Sun, R. J. Orazi, and S. A. Pappert, *IEEE Photon. Technol. Lett.*, vol. 8, pp. 154-156, 1996.
5. R. Helkey, J. C. Twinchell, and C. H. Cox, *J. Lightwave Technol.*, vol. 15, pp.956-961, 1997.
6. H. Roussell, R. Helkey, *IEEE Microwave Guided Wave Lett.*, vol. 8, pp. 408-410, 1998.
7. C. P. Liu, A. J. Seeds, and D. Wake, *IEEE Microwave Guided Wave Lett.*, vol. 7, pp. 72-74, 1997.
8. Y. Betser, D. Ritter, C. P. Liu, A. J. Seeds, and A. Madjar, *J. Lightwave Technol.*, vol. 16, pp. 605-609, 1998.
9. Y. Betser, J. Lasri, V. Sidorov, S. Cohen, D. Ritter, M. Orenstein, G. Eisensein, A. J. Seeds, and A. Madjar, *IEEE Trans. Microwave Theory Tech.*, vol. 47, pp. 1358-1364, 1999.
10. R. B. Welstand, S. A. Pappert, C. K. Sun, J. T. Zhu, Y. Z. Liu, and P. K. L. Yu, *IEEE Photon. Technol. Lett.*, vol. 8, pp. 1540-1562, 1996.
11. K. K. Loi, J. H. Hodiak, W. B. Mei, C. W. Tu, W. S. C. Chang, D. T. Nichols, L. J. Lembo, and J. C. Brock, *IEEE Photon. Technol. Lett.*, vol. 10, pp. 1572-1574, 1998.
12. C. K. Sun, S. A. Pappert, R. B. Welstand, J. T. Zhu, P. K. L. Yu, Y. Z. Liu, and J. M. Chen, *Electron. Lett.*, vol. 31, pp. 902-903, 1995.
13. G. L. Li, Y. Z. Liu, R. B. Welstand, C. K. Sun, W. X. Chen, J. T. Zhu, S. A. Pappert, and P. K. L. Yu, *IEEE Photon. Technol. Lett.*, vol. 11, pp.659-61, 1999.

Analysis of the Multi-Electrode Linearized EA modulator

Y. Zhuang, G. L. Li, W. S. C. Chang, P. K. L. Yu,
Department of Electrical and Computer Engineering
University of California, San Diego
La Jolla, CA 92093-0407

Y. Z. Liu,
Fermionics Lasertech
1153 Lawrence Drive, Newbury Park, CA 91320

ABSTRACT

A new approach for linearizing electroabsorption modulators (EAM) is presented here. It will be very useful for broadband, analog, radio frequency fiber-optic links. In this approach, two or more EAM will be fabricated in series on the same waveguide. Theoretical analysis shows that cancellation of both the second order and third order harmonic distortions can be obtained simultaneously by using proper electrode length and by biasing appropriately the electrodes, leading to an enhancement of the multi-octave spurious free dynamic range (SFDR). Simulation shows that the SFDR of the optical link for the two-electrode case is 10dB larger than that for a single electrode case. Experimental confirmation of the theoretical prediction on distortion reduction is also presented.

Keywords: Electroabsorption modulator, Harmonic distortion, Spurious free dynamic range.

1. INTRODUCTION

Transmission of microwave and millimeter-wave signal via analog fiber-optical links has widespread applications in antenna remoting and RF distribution systems. It has a number of advantages over conventional microwave links such as low transmission loss at high frequencies, compactness, wide-bandwidth, high degree of security, and immunity to electromagnetic interference etc. For such RF photonic links, EA modulator will play a key role because it has low chirp, low modulation voltage and large bandwidth. However, low-harmonic distortion is required in order to obtain large SFDR. The harmonic distortion of EAM must be minimized.

Recent work for linearization of modulators includes electrical pre-distortion [1] & [2], dual wavelength [3] or other optical feed-forward compensation schemes [4]-[6]. It is difficult to extend electrical pre-distortion scheme to high microwave frequencies. Dual wavelength scheme requires additional optical components and wide optical wavelength span for the link. The feed-forward compensation approaches are hard to implement for EAM.

In this paper, we propose a new linearized design of EAM by using two or more electrodes fabricated in tandem. Fig.1 illustrates the two-electrode case. Different biases are applied on the two electrodes. By properly choosing the biases and the electrode lengths, certain orders of non-linearity can cancel each other. Thus the SFDR of the RF optical fiber link can be increased. Theoretical analysis and simulation results of two electrodes in tandem are presented in the following sections.

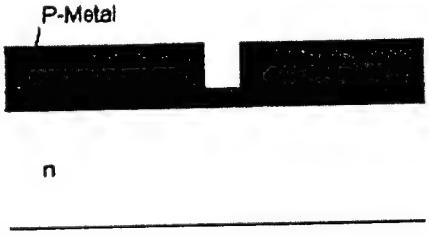

Fig. 1 Structure of two-electrode Modulator.

The linearization technique involved in this paper can also apply to two dissimilar modulators in tandem. Experimentally, we have demonstrated the distortion cancellation effect using one EA modulator and one Mach-Zehnder in series. Cancellation of harmonics is obtained by changing the biases of these two modulators.

2. THEORETICAL ANALYSIS

2.1. The transmission function of the two-electrode EAM

The transmission function of the one-electrode EA modulator is modeled as:

$$T = e^{-\Gamma \alpha L}$$

Here, Γ is the optical confinement factor of the absorption layer,
α is the optical absorption coefficient of the absorption layer,
L is the optical waveguide length.

And $\alpha = \alpha_b + \Delta\alpha$, where α_b is absorption coefficient at DC bias V_b, $\Delta\alpha$ is the change of α in the material due to the RF voltage V_{RF}.

In the two-electrode scheme, we break the electrode L into two sections. It is equivalent to two electroabsorption modulators under different DC bias connected in series. The same V_{RF} is applied to both electrodes. The total transmission function is the product of the two transmission functions.

$$T = e^{-\Gamma \alpha_1 L_1} \cdot e^{-\Gamma \alpha_2 L_2} \qquad (1)$$

Here, $\alpha_1 = \alpha_{b1} + \Delta\alpha_1$, α_{b1} is the absorption coefficient at DC bias V_{b1},

$\alpha_2 = \alpha_{b2} + \Delta\alpha_2$, α_{b2} is the absorption coefficient at DC bias V_{b2},

L_1 is the length of the first electrode biased at V_{b1},
L_2 is the length of the second electrode biased at V_{b2},
$L = L_1 + L_2$.

2.2. Harmonic distortions of the two-electrode modulator

If Taylor expansion is applied to the transmission function in Eq. (1) at the DC bias points V_{b1} and V_{b2},

We get T= $T|_{V_{RF}=0} + \sum_k (V_{RF} \sin \omega t)^k \cdot h_k$ (2)

Here, $h_k = \frac{1}{k!}\left(\frac{\partial^k T}{\partial V^k}\right)\Big|_{V=V_{b1},V_{b2}}$. It's the coefficient of the $\sin \omega t$ to the k^{th} power. $(\sin \omega t)^k$ yields sinkωt, i.e. the kth harmonic, and other lower harmonic terms. h_k is not equivalent to the total magnitude of the k^{th} harmonic because higher order harmonics may also contribute to the k^{th} harmonic. But the higher order contributions to k^{th} harmonics are relatively small comparing with the contribution of $(\sin \omega t)^k$.

From equation (2), we obtain the following results:

(1) When

$$L_1 \frac{\partial^2 \alpha_1}{\partial V^2}|_{Vb1} + L_2 \frac{\partial^2 \alpha_2}{\partial V^2}|_{Vb2} = \Gamma (L_1 \frac{\partial \alpha_1}{\partial V}|_{Vb1} + L_2 \frac{\partial \alpha_2}{\partial V}|_{Vb2})^2 \qquad (3)$$

h_2=0.

(2) When

$$\begin{cases} L_1 \frac{\partial^2 \alpha_1}{\partial V^2}|_{Vb1} + L_2 \frac{\partial^2 \alpha_2}{\partial V^2}|_{Vb2} = \Gamma (L_1 \frac{\partial \alpha_1}{\partial V}|_{Vb1} + L_2 \frac{\partial \alpha_2}{\partial V}|_{Vb2})^2 \\ L_1 \frac{\partial^3 \alpha_1}{\partial V^3}|_{Vb1} + L_2 \frac{\partial^3 \alpha_2}{\partial V^3}|_{Vb2} = 2\Gamma^2 (L_1 \frac{\partial \alpha_1}{\partial V}|_{Vb1} + L_2 \frac{\partial \alpha_2}{\partial V}|_{Vb2})^3 \end{cases} \quad (4)$$

$h_2=0$ and $h_3=0$.

(3) Similar relationships exist for $h_2=h_3=h_4=0$ and for $h_2=h_3=h_4=h_5=0$.

Although there are four parameters (L_1, L_2, V_{b1}, V_{b2}), since $L_1+L_2=L$ there are only three parameters that we can choose freely. For example, according to equation (4), $h_2=0$ and $h_3=0$ at the same time for the three properly chosen free parameters. Amplitude of the nth harmonic contains contributions from h_n and h_k (k>n). Complete cancellation of harmonics will occur only when contributions from orders higher than k can be neglected. This approximation breaks down whenever h_k is small. In addition, the range of bias voltages and electrode lengths for cancellation of any given order of harmonic is very narrow. Therefore, in practice there is only reduction of harmonics, but not complete cancellation of harmonics. It is also interesting to note that, in practical links, we are interested more in the third order intermodulation distortion than harmonic distortion. However, the formula for intermodulation distortion is much more complicated than for harmonic distortion. Therefore, only the analysis for harmonic distortion is presented here. We expect that there will be a corresponding reduction of kth order intermodulation distortion whenever there is a reduction of kth order harmonic distortion.

2.3. The SFDR of the link

At the detector output, let the RF signal power be P_1, the power of the 2nd harmonic be P_2, and the power of the 3rd harmonic be P_3. Let the noise power be N. The $SFDR_n$ of the link (due to the nth harmonic) is the range of P_1 that varies from the minimum at $P_1=N$ to the maximum at $P_n=N$. Let m be the modulation depth which is the ratio of P_1 to the DC bias optical power. $10\log_{10}(N/P_1)$ is the noise power expressed in dBc. $10\log(P_n/P_1)$ is the nth harmonic power expressed in dBc. $SFDR_n$ is the range in dBc, from 0 dBc (corresponding to $N/P_1=1$) to the intersection of the $10\log(N/P_1)$ line with the $10\log(P_n/P_1)$ line at a larger modulation index m. Fig. 2 illustrates how we find $SFDR_n$. The $SFDR_n$ is different for different order of distortion. Then the broadband SFDR of the link is the smallest one of all the $SFDR_n$.

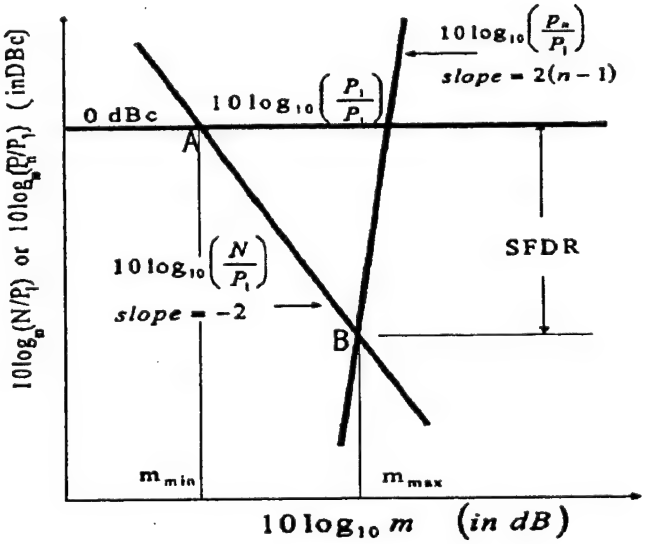

Fig. 2 SFDR of the link.

If 2nd and 3rd order harmonics (related to h_2 and h_3) are reduced, the power P_2 and P_3 will reduce. This will make the 10 $\log_{10}$ (P_2/P_1) line and 10 $\log_{10}$ (P_3/P_1) line in Fig. 2 move downward. The intersection point B of the 10 $\log_{10}$ (N/P_1) line with the 10 $\log_{10}$ (P_n/P_1) line will also move down. The SFDR is increased.

In numerical calculation, we see that as h_2 and h_3 decrease, h_4 and h_5 also increase. The increase of h_4 and h_5 eventually limits the overall SFDR improvement.

3. SIMULATION RESULTS

In order to illustrate the analysis given in section 2, let us consider first the simplest case $L_1=L_2=L/2$. We will show that the simulated SFDR of the link with a two-electrode modulator is significantly larger than that of the one-electrode case. $(\sin\omega t)^4$ and $(\sin\omega t)^5$ contributions to the fundamental, 2nd harmonic and 3rd harmonic are included. Other higher order contributions are neglected.

Two types of EAM are simulated. One uses the bulk material which exhibits Franz-Keldysh effect (FKE), the other one uses Multiple Quantum Well (MQW) material.

3.1. For modulator using Franz-Keldysh effect

The absorption coefficient data used here is from theoretical calculation. The wavelength is 1.55μm and the detuning energy is 54meV.

The assumptions used in the simulation are:

Optical input power = 15dBm;
Modulator insertion loss = 10 dB;
Optical confinement factor = 0.55;
Length L (for both modulators) = 200 μ m;
Detector responsivity = 0.75 A/W;
Internal resistance of RF source and load = 50 ohms;
Noise floor = –160dBm/Hz.

The SFDR of the two-electrode modulator (taking into account of both 2nd and 3rd harmonics) is shown in Fig. 3(a) & 3(b). Fig. 3(b) is a magnified figure of Fig. 3(a) for the range $1.6V>V_{b1}>1.2V$ and $1.2V>V_{b2}>0.8V$. Fig 3(a) & 3(b) are contour maps of SFDR, the two axes are the DC bias voltages for two electrodes. The SFDR of the one-electrode modulator is shown in Fig. 3(c). In Fig. 3(c), the x-axis is the DC bias voltage, the y-axis is SFDR. From Fig. 3(b) it is clear that the best DC biases for the two-electrode modulator are $V_{b1}=1.412V$, $V_{b2}=0.910V$. Under these biases, the 2nd and 3rd harmonics are both very small, and the fundamental is reduced only slightly from the fundamental of the one-electrode case. Table1 is the comparison of two-electrode modulator and one-electrode modulator.

Table 1

	DC bias	SFDR	h_1
Two-electrode	$V_{b1}=1.412V$ $V_{b2}=0.910V$	104.2dBc	-0.33
One-Electrode	$V_b=1.161V$ (2nd order null point)	95.0dBc	-0.34

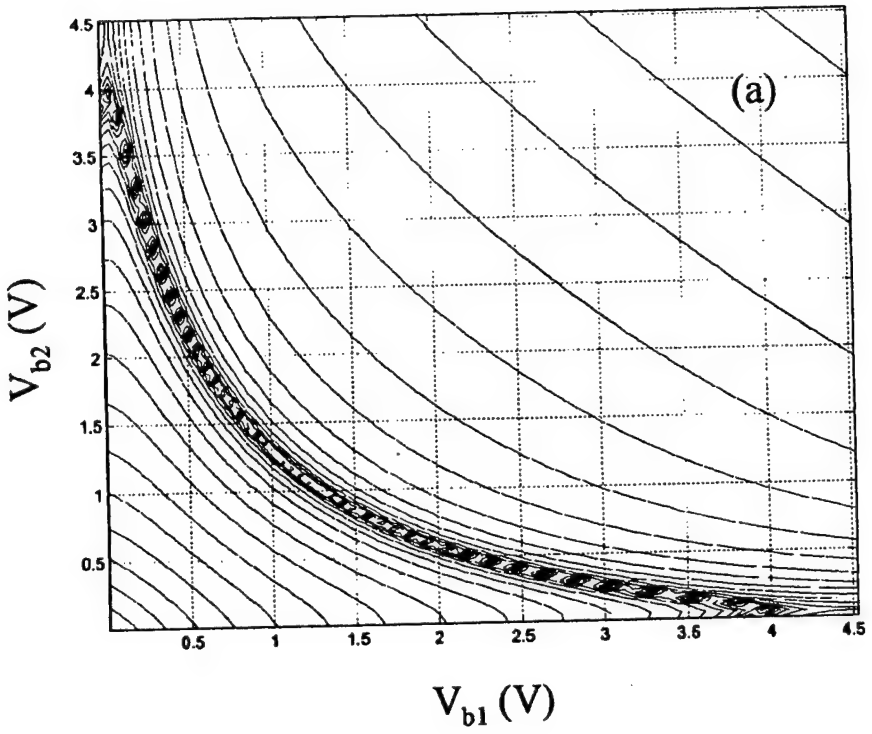
(a)
4.5
4
3.5
3
2.5
2
1.5
1
0.5
0.5
1
1.5
2
2.5
3
3.5
4
4.5
V_{b2} (V)
V_{b1} (V)

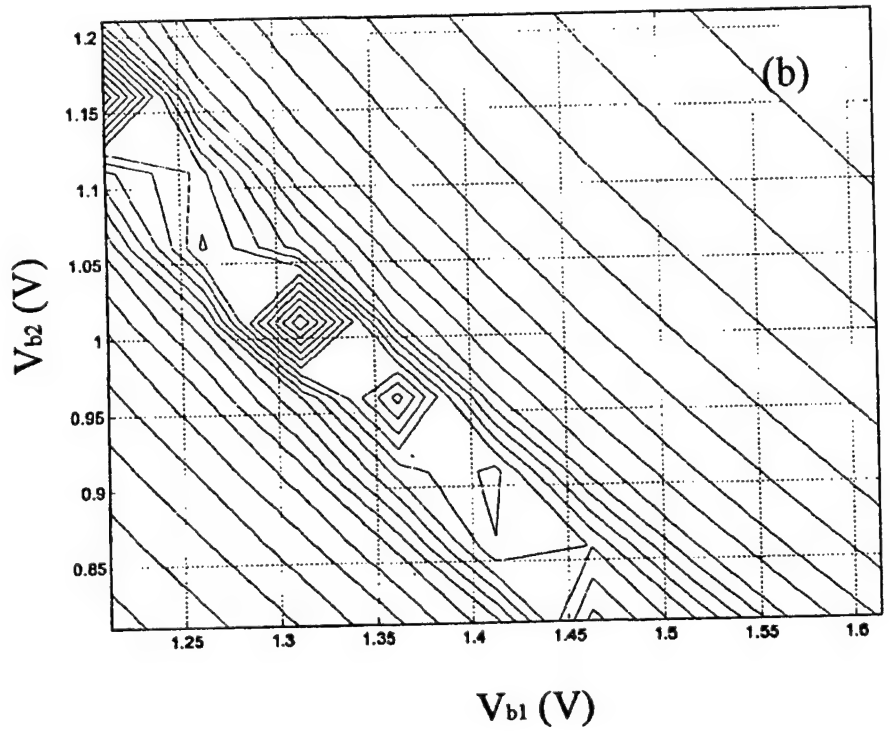
(b)
1.2
1.15
1.1
1.05
1
0.95
0.9
0.85
1.25
1.3
1.35
1.4
1.45
1.5
1.55
1.6
V_{b2} (V)
V_{b1} (V)

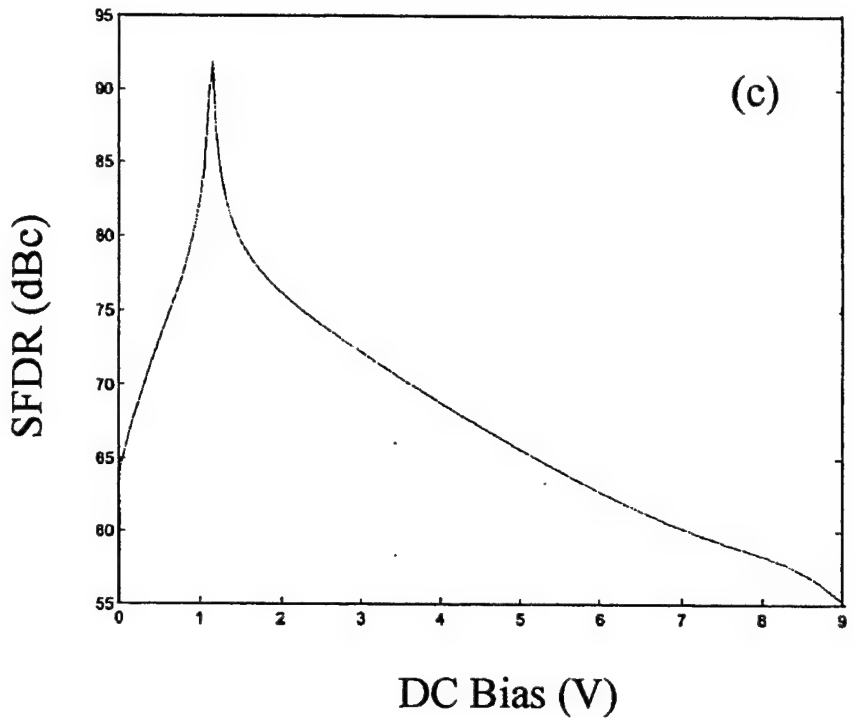

Fig. 3 Comparison of SFDR of two-electrode and one-electrode modulator.
(a) and (b) are for two-electrode modulator; (c) is for one-electrode modulator.

3.2. For multiple quantum well (MQW) EAM

The absorption coefficient data used here is from the experimental transmission curve [7]. The active layer of this MQW EAM is InAsP-GaInP. The operation wavelength is 1.32μm and detuning energy is 22meV.

The assumptions used in the simulation are:

Optical power = 10dBm;
Modulator insertion loss = 8dB;
Length L (for both modulators) = 185um;
Detector responsivity = 0.89A/W;
Noise floor = -160dBm/Hz.

Table 2 shows the comparison of two-electrode modulator and one-electrode modulator. For the two-electrode modulator, V_{b1}=0.82V & V_{b2}=0.49V are the best DC biases for maximizing the SFDR. For the one-electrode case, V_b=0.72V is the best bias point for maximizing the SFDR.

Table 2

	DC bias	SFDR	h_1
Two-electrode	V_{b1}=0.82V V_{b2}=0.49V	102.4dBc	-1.11
One-Electrode	V_b=0.72V (2^{nd} order null point)	93.3dBc	-1.17

From simulation results shown in Table 1 & 2, the SFDR of the two-electrode modulator for both FKE and MQW EAM can be increased by about 10dB as compared to a single-electrode modulator.

Similar simulations have been performed for two-electrode modulators with unequal lengths ($L_1 \neq L_2$). We can improve the SFDR even more by adjusting L_1 and L_2. However, the increase in h_4 and h_5 will limit the SFDR improvement. Comparing with the results obtained for the equal length case, the difference is minor, just about 3~4 dBc.

4. EXPERIMENTAL RESULTS

The cancellation technique for harmonics in two-electrode modulator shown in section 2 & 3 is also applicable to two dissimilar modulators in tandem. For demonstration purpose, we use one FKE EA modulator and one Mach-Zehnder modulator in series to demonstrate the distortion cancellation effect.

The experimental set-up is shown in Fig.4.

The laser power = 18dBm;
Input RF power for both the MZM and the EAM = 8dBm;
Input RF frequency = 1GHz.

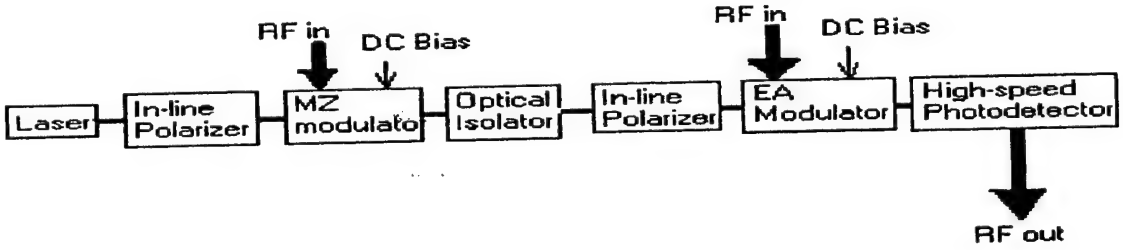

Fig.4 Measurement set-up.

The measured fundamental, 2nd ad 3rd harmonics are shown in table 3 for various combinations of V_{b1} and V_{b2}.

Table 3

DC Bias for MZM V_{b1} (V)	4.82	4.82	4.98	5.04	5.27	5.48
DC Bias for EAM V_{b2} (V)	-1.89	-1.41	-1.50	-1.50	-1.51	-1.50
Fundamental output @1GHz (dBm)	-63.20	-64.34	-64.11	-65.31	-66.48	-64.61
2nd Harmonic @ 2GHz (dBm)	-83.90	-77.50	-78.52	-80.52	-84.08	-83.47
3rd Harmonic @ 3GHZ (dBm)	-81.49	-82.24	-83.35	-84.59	-89.42	-93.46

We see that the largest fundamental signal is obtained at V_{b1}= 4.82V & V_{b2}= -1.89V. The best cancellation of third harmonic happens at V_{b1}=5.48V & V_{b2}= -1.50V. Comparing these two cases, the cancellation of 3rd order harmonic is about 12dB. The 2nd order harmonic is about the same. The fundamental drops about 1.5dB.

5. CONCLUSION

Simulation results show that the two-electrode modulator scheme can improve the broadband SFDR of an optical link about 10 dB, with just a slight drop of the fundamental signal.

Experimentally, the data collected from MZM and EAM in tandem show a decrease of 12dB in 3rd order harmonic with almost no change in 2nd harmonic and only 1.5dB penalty in reduction of fundamental signal.

The narrow range of bias voltages within which larger cancellation of 2nd and 3rd harmonics may take place and the increase in higher order h_k coefficients may limit the improvement in broadband SFDR that can be obtained by more complex distortion cancellation schemes.

ACKNOWLEDGMENT

The authors would like to thank Dong-Soo Shin and Yang Wu at University of California , San Diego for their help. This work is partially sponsored by SPAWAR and United States AFRL.

References

1. G.C.Wilson, T.H.Wood, J.L. Zyskind, J.W. Sulhoff, S.B. Krasulick, J.E. Johnson, T. Tanbun-Ek, and P.A. Morton, "Analogue Transmission at 1.55μm using Linearised Electroabsorption Modulator/DFB Lasers and Fiber Amplifier", *Electron. Lett.*, Vol. 31, No. 22, pp.1934-1935, 1995;
2. T.Iwai and K.Sato, " Dispersion-included Distortion in AM-SCM Transmission Systems Employing Linearised MQW-EA Modulator", *Electron. Lett.*, Vol. 31, No. 15, pp1272-1273, 1995.
3. K.K.Loi, J.H.Hodiak, X.B.Mei, C.W.Tu, W.S.C.Chang, "Linearization of 1.3-μm MQW Electroabsorption Modulators Using an All-Optical Frequency-Insensitive Technique", *IEEE Photonics Technology Letters*, Vol. 10, pp. 964-966, July 1998;
4. M.Shin, J.Lim, C.Y.Park, J.Kim, J.S.Kim, K.E.Pyun, S.Hong, "High-Speed Linear Analog Multiple Quantum Well Electroabsorption Modulator Integrated with MMI Couplers", *IEEE MWP'99 Digest*, pp.25-28. 1999;
5. Myunghun Shin and songcheol Hong, "A Novel Linearization Method of Multiple Quantum Well (MQW) Electroabsorption Analog Modulator", *Japanese Journal of Applied Physics*, Vol. 38, pp.2569-2572 April 1999;
6. S.A.Hamilton, D.R.Yankelevich, A.Knoesen, R.T.Weverka, R.Hill, "Comparison of an In-Line Asymmetric Directional Coupler Modulator with Distributed Optical Loss to Other Linearized Electrooptic Modulator", *IEEE Transactions on Microwave Theory and Techniques*. Vol. 47, No.7, pp.1184-1193. July 1999;
7. D.S. Shin, G.L. Li, C.K. Sun, S.A. Pappert, K.K. Loi, W.S.C. Chang and P.K.L. Yu, "Optoelectronic RF Signal Mixing Using an Electroabsorption Waveguide as an Integrated Photodetector/Mixer", *IEEE Photonics Technology Letters*, Vol. 12, No. 2, February 2000.

Design and Fabrication of Traveling Wave Electroabsorption Modulator

G. L. Li, D. S. Shin, W. S. C. Chang, P. M. Asbeck and P. K. L. Yu
Dept. of Electrical and Computer Engineering
University of California, San Diego, La Jolla, CA 92093-0407

C. K. Sun, S. A. Pappert, R. Nguyen
Space & Naval Warfare Systems Center, Point Loma, CA 92151

SUMMARY

Semiconductor electroabsorption modulator (EAM) is a promising alternative to lithium niobate modulator for digital and analog fiber optic links due to its inherent small size, high modulation efficiency, and potential of monolithic integration with other electronic and optoelectronic components. For high-speed application, the bandwidth of the lumped element EAM is known to be RC-time limited. To achieve an ultra large bandwidth in lumped element EAM, the modulation efficiency has to be greatly sacrificed. This is especially critical in analog operation where RF link loss and noise figure must be minimized. To overcome the RC bandwidth limit and to avoid significantly compromising the modulation efficiency, the traveling wave electroabsorption modulator (TW-EAM) has been proposed and experimentally investigated by several authors [1-5].

In our previous work [5], detailed theoretical analysis and numerical calculations have been carried out for ultra high-speed (>50 GHz) TW-EAM, including effects of velocity mismatch, impedance mismatch and microwave attenuation. It was found that due to the optical propagation loss of the waveguide, the TW-EAM waveguide length for maximum RF link gain is limited to 200 ~ 300 μm. A quasi-static equivalent circuit model was used to examine the TW-EAM microwave properties, including the effect of photocurrent. Three TW-EAM design approaches were discussed: low impedance matching; reducing the waveguide capacitance; and distributing the modulation region.

Following the previous analysis, we have designed and fabricated TW-EAM devices using low impedance matching approach. Figure 1 shows the cross section of the device. The TW-EAM optical waveguide is similarly designed as that of the lumped element EAMs [6]. Its microwave design is more critical and deserves a more thorough discussion.

The equivalent circuit model, illustrated in Figure 2, is very helpful in understanding the TW-EAM microwave design. In this circuit model, R_{con} is the conduction resistance, L_m is the inductance, R_S is the device series resistance, C_m is the

junction capacitance, R_O is the equivalent ac resistance due to the dependence of the EAM photocurrent on the junction voltage. These circuit parameters determine the TW-EAM frequency response [5]. To achieve ultra large bandwidth, small C_m, R_S and R_{con} are desirable. However, the effect of inductance L_m is not so straightforward to predict. This

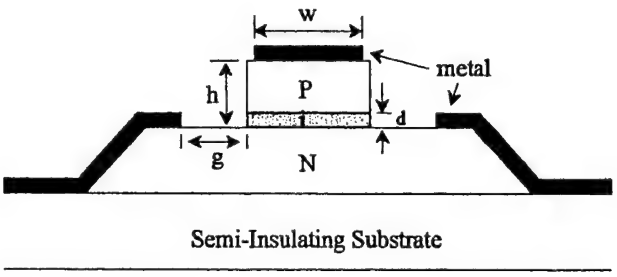

Figure 1. Cross-section of the TW-EAM device.

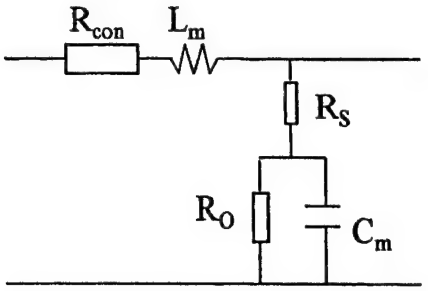

Figure 2. Quasi-static circuit model for a unit length of TW-EAM transmission line.

is illustrated in Figure 3. When the terminator impedance $Z_L > 50\ \Omega$, the waveguide inductance will have little impact on the TW-EAM bandwidth; when $Z_L = 22\ \Omega$, in the L_m range of 0.1 nH/mm to 1.0 nH/mm, a larger L_m will yield a larger bandwidth. This suggests that in our device design which uses a low impedance matching approach, a larger inductance L_m would be preferred.

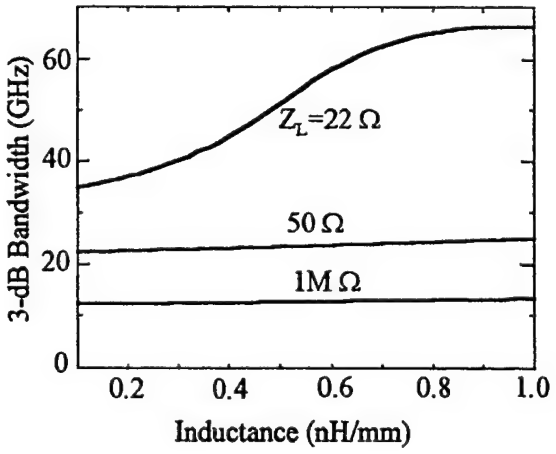

Fig. 3. Effect of waveguide inductance on the 3-dB bandwidth.

The values of all above circuit parameters are determined by the structure design in Figure 1. The

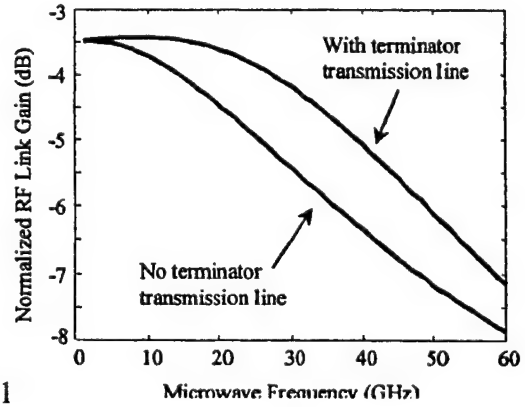

capacitance C_m depends upon the waveguide width and the intrinsic layer thickness, which have been determined in the optical waveguide design for maximum modulation efficiency. To achieve a larger inductance, L_m, a smaller central metal width, w, a larger electrode gap, g, and a larger waveguide height, h, are preferred. However, smaller w causes larger R_{con}; larger g and larger h cause larger R_S. Detail numerical calculations are needed in order to optimize these structure geometry parameters to obtain the largest bandwidth.

In order to connect the low impedance terminator to the TW-EAM waveguide, a microwave transmission line is needed. This transmission line design could have a significant impact to the TW-EAM frequency response. In the calculation we can treat this transmission line plus the terminator as an equivalent terminator. The impedance of this equivalent terminator has an imaginary part that is frequency dependent, which is similar to the TW-EAM waveguide impedance [5]. This infers that a better impedance matching could be achieved by a proper design of the terminator transmission line. However, the transmission line length and impedance have to be optimized in order to get benefit on the TW-EAM bandwidth. More than 10 GHz bandwidth improvement can be obtained with the effect of terminator transmission line, as is illustrated in Figure 4.

The device fabrication proceeds in the conventional manner. Our prior work uses dry etching (RIBE or RIE) that creates much waveguide sidewall roughness, presently we use wet chemical etching. However, chemical etching usually produces trapezoidal etching profile, which increases the device capacitance. With judiciously chosen etchant and etching conditions, we have successfully obtained a quasi-rectangular waveguide cross-section.

In the lithographic step that connects the metal on top of the waveguide to the bottom electrode on the semi-insulating substrate, extra caution should be exercised, as there are several micrometers difference in height between them. We have presently overcome this difficulty through the use of multiple lithography and specially designed masks.

In this work, we have designed and fabricated traveling wave electroabsorption modulators based on our previous analysis. Some important issues on the design and fabrication will be discussed during the presentation, together with the measurement results.

Acknowledgment: This work is partially funded by DARPA, ONR and MICRO-Raytheon program.

References:

1. K. Kawano, M. Kohtoku, M. Ueki, T. Ito, S. Kondoh, Y. Noguchi and Y. Hasumi, *Electron. Lett.*, vol. 33, pp. 1580-1581, 1997.
2. H. H. Liao, X. B. Mei, K. K. Loi, C. W. Tu, P. M. Asbeck and W. S. C. Chang, *Proc. SPIE, Optoelectronic Integrated Circuits,* vol. 3006, pp. 291-300, 1997.
3. S. Z. Zhang, Y. J. Chiu, P. Abraham and J. E. Bowers, *IEEE Photon. Technol. Lett.*, vol. 11, pp.191-193, 1999.
4. W. S. Cho, Y. S. Lim and Y. W. Choi, *MWP'99 digest,* pp. 153-156, 1999.
5. G. L. Li, C. K. Sun, S. A. Pappert, W. X. Chen and P. K. L. Yu, *IEEE Trans. on Microwave Theory and Techniques*, vol. 47, pp. 1177-1183.1999.
6. G. L. Li, R. B. Welstand, W. X. Chen, J. T. Zhu, S. A. Pappert, C. K. Sun, Y. Z. Liu and P. K. L. Yu, *IEEE Photonics Technol. Letts.*, vol.10, pp.672-674, 1998.

Performance of the Electroabsorption Modulator as an Integrated Optoelectronic Mixer for RF Frequency Conversion

D. S. Shin, G. L. Li, C. K. Sun*, S. A. Pappert*, W. S. C. Chang, and P. K. L. Yu
University of California, San Diego; Department of ECE; La Jolla, CA 92093-0407
* SPAWAR Systems Ctr.; San Diego, CA 92152-5001

Abstract: We present the performance of the multiple-quantum-well and Franz-Keldysh electroabsorption waveguides as an integrated photodetector/mixer for frequency conversion of RF signals. The InAsP/GaInP multiple-quantum-well waveguide exhibits a low phase noise and large SFDR conversion.

Summary

Microwave photonics is considered to be a viable alternative technology in some application areas where electronics has traditionally played a central role. Frequency converting photonic links for antenna remoting applications is an example of this where antenna front-end hardware complexity can be reduced and the deleterious effects of fiber dispersion may be avoided [1,2]. Many of the conversion schemes take advantage of the optical local oscillator (LO), which is less complex than the electronic LO at high frequency, and has shown lower phase noise [3]. There have been several proposals to achieve low conversion loss and large spur-free dynamic range (SFDR) for photonic frequency converting links [4-6]. One approach makes use of Mach-Zehnder modulators (MZM's) at very high optical LO power (350 mW) to achieve positive link conversion gain [5,6]. An alternative approach uses either a heterojunction phototransistor or heterojunction bipolar transistor (HBT) to convert the modulated optical radiation to the RF signal, by using the inherent nonlinearity of the device [7-9]. In [8], a 10.4-dB intrinsic conversion gain (-5.5 dB external conversion gain) was achieved using an electrical LO. In [9], two HBT's in a cascode configuration were used to achieve an intrinsic conversion gain of 18.2 dB and an extrinsic conversion gain of 7.4 dB with a three-stub tuner.

In a prior work [10], we have proposed and demonstrated an alternate RF signal conversion approach using an electroabsorption (EA) waveguide as a photodetector/mixer. In this approach, frequency converted *electrical* RF signals from the EA waveguide, operating as an optoelectronic mixer (OEM), is generated and made available for subsequent signal processing. The down-converted RF signal can be sent through conventional electrical cable that has low attenuation at baseband/IF frequency. We have demonstrated a moderate conversion loss and high SFDR, RF signal mixing using moderate optical LO power and a simple system configuration [10].

In this work, we compare the performance of the multiple-quantum-well (MQW) and Franz-Keldysh effect (FKE) EA-OEM in this conversion scheme.

In EA waveguides, the electroabsorption process generates an electric-field dependent photocurrent, $I_{ph}(V, P_{opt}) = \eta_m(V) P_{opt}$, where P_{opt} is the optical power and $\eta_m(V)$ is the modulator's detection responsivity. η_m is dependent on the applied bias (therefore, the electric field), and is independent of optical power provided that the device is operated below saturation. When a DC optical power, P_0, and modulation optical power, p at ω_{LO}, are incident on an EA waveguide driven by a DC bias voltage, V_b, along with a RF signal voltage, v at ω_s, the photocurrent generated at the device is given by:

$$I_{ph}(V, P_{opt}) = \eta_m(V_b + v\cos\omega_s t)\cdot(P_0 + p\cos\omega_{LO} t) \quad (1)$$

The up-and down-converted signals at $\omega_s \pm \omega_{LO}$ are obtained from a small signal analysis of $\eta_m(V_b + v\cos\omega_s t)$ as:

$$I_{ph}^{mix} = \frac{1}{2}\frac{d\eta_m}{dV}\bigg|_{Vb} vp\cos(\omega_s \pm \omega_{LO})t \qquad (2)$$

The higher order derivatives of η_m contribute to the harmonic and intermodulation distortions of this OEM. Note from $d\eta_m/dV|_{Vb}$ in (2) that the electroabsorption is crucial in generating the mixed signals. This distinguishes the electro-absorption mode of the EA-OEM from the usual *pin* photodetection where the responsivity is constant with voltage.

We first compare the current that gives the mixed signals detected by the remote detector, when the EAM is used as a modulator, to the integrated mixer photocurrent. The remote detector photocurrent can be expressed as $I_{trans} = \eta_d P_{opt} t_{ff} T(V)$ where η_d is the responsivity of the remote detector, t_{ff} is the transmission factor of the EAM, and $T(V)$ is the transfer function of the EAM normalized to the incident optical power. The corresponding photocurrent that gives the mixing of ω_s and ω_{LO} is:

$$I_{trans}^{mix} = \frac{1}{2}\eta_d t_{ff}\frac{dT}{dV}\bigg|_{Vb} vp\cos(\omega_s \pm \omega_{LO})t \qquad (3)$$

From I_{ph}^{mix} with I_{trans}^{mix}, the RF power of the converted signals can be obtained, assuming a 50-Ω load resistor. The ratio of powers of the frequency-converted signals in these two cases can be expressed in dB as:

$$Ratio = 20Log\left(\frac{I_{ph}^{mix}}{I_{trans}^{mix}}\right) = 20Log\left(\frac{dI_{ph}/dV}{dI_d/dV}\right) \qquad (4)$$

Here I_{ph} and I_d are the photocurrent detected at the EA-OEM and the remote detector, respectively, and the derivatives are evaluated at the modulator bias, V_b.

In the experiment, AR coated strain-compensated InAsP/GaInP MQW EA waveguide that utilizes the quantum-confined Stark effect [11] and an InGaAsP/InP waveguide [12] that used the Franz-Keldysh effect were compared. The MQW sample has 8 periods of 8.9-nm thick compressively-strained InAsP wells and 7.4-nm thick tensile-strained GaInP barriers, sandwiched by InGaAsP cladding layers. At λ = 1.319 μm, the transmission (as detected by a remote detector with 0.89-A/W responsivity) and photocurrent characteristics vs. DC bias of the two devices are shown in Fig. 1a and Fig 1b.

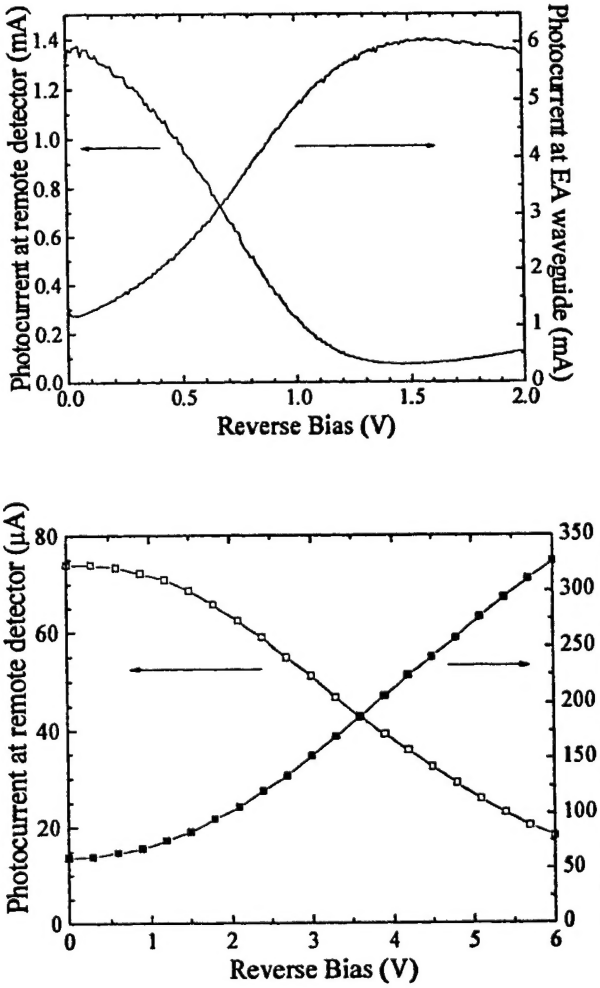

Fig. 1.Transmission and absorption characteristics of (a) the MQW (at 10 mW), (b) bulk InGaAsP waveguides (at 1 mW).

The normalized slope efficiencies are -1.1 V^{-1} and -0.18 V^{-1}, respectively, for these transmission curves. The fiber-to-fiber insertion loss of the waveguides are 8.0 dB and 11 dB, respectively.

The RF-frequency-mixing setup is shown in Fig. 2 [10] with two Nd:YAG lasers generating a beat tone at a 100-% modulation depth, which was used as an optical LO signal to the EA waveguide. Electrical voltage that contained the DC bias as well as the RF signal at ω_s was applied to the EA-OEM under test.

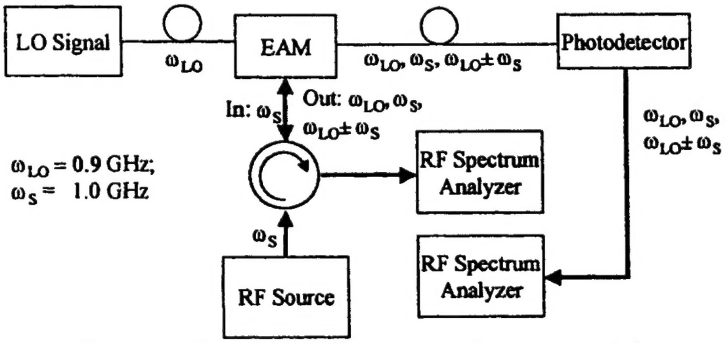

Fig. 2. Experimental set-up for the mixing experiment using the EA waveguide.

The DC bias was first set at the second order null point of the transmission curve, which corresponds to the highest slope efficiency of the photocurrent vs. DC bias curve. When the RF signal power was increased from –20 dBm to –10 dBm, the converted signal powers increased by 10 dB. They closely follow the behavior predicted by (2). The MQW EA waveguide became saturated around 10-mW of LO optical power.

Defining the conversion loss as the ratio of the input RF signal power to the output frequency converted signal power, the conversion loss for the case when the MQW EA-OEM was used as a photodetector/mixer is measured at 18.9 dB. This conversion loss is mainly limited by LO optical power (10 mW) and the saturation power of the MQW waveguide. When this MQW EA waveguide was used as a modulator/mixer and the converted signals were transmitted through the optical fiber as in [4-6], the conversion loss was increased to 27.8 dB. The increase in conversion loss is mainly due to the fact that the responsivity of the remote detector, η_d at the end of the fiber link combined with the EA waveguide insertion loss, t_{ff}, was much smaller than that of the EA waveguide.

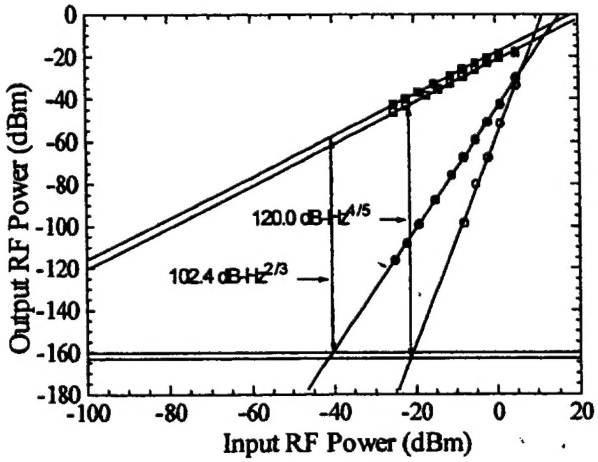

Fig. 3. Two-tone test of the MQW EA photodetector/RF mixer. Converted RF signals (■: for highest slope point, □: for third-order null point) and the IMD_3's (●: for highest slope point, ○: third-order null point) are shown.

Two-tone SFDR measurement was carried out with the RF tones at 1.00 and 1.02 GHz and the optical LO tone at 0.90 GHz: The converted signals and the their third-order intermodulation distortions (IMD_3's) were measured. (Due to the bandwidth limitation of the circulator, only the up-converted signals were measured.) When the MQW EA waveguide was biased at the highest slope point of the device photocurrent vs. DC bias curve (second-order null point), a SFDR of 102.4 dB-Hz$^{2/3}$ was obtained at 10-mW optical LO power for the up-converted signal at 1.90 GHz. When the MQW EA-OEM was biased at the third-order null point of the device photocurrent vs. DC bias curve, the up-converted RF signal power was reduced by ~3 dB, but the sub-octave SFDR was measured at 120.0 dB-Hz$^{4/5}$ with the fifth-order dependence on the input RF power. At the third-order null point, the IMD_3 due to the third-order input power dependence becomes null, making the IMD_3 depending on the next order, which is the fifth order. The results are shown in Fig. 3.

For the InGaAsP FKE EA-OEM, a larger RF conversion loss (29.2 dB) was measured at the same LO optical power of 10 mW, mainly due to the smaller slope efficiency of the FKE. However, the single-octave SFDR's of this photodetector/mixer are within 4 dB of those of the above MQW device, primarily due to the lower degree of saturation of the FKE device at 10 mW. These results are summarized in Table 1.

Device	Conversion loss (dB)	SFDR
InAsP/GaInP MQW	18.9 (2^{nd} order null) 21.9 (3^{rd} order null)	102 dB-$Hz^{2/3}$ 120 dB-$Hz^{4/5}$
Bulk InGaAsP	29.2 (2^{nd} order null) 33.2 (3^{rd} order null)	98 dB-$Hz^{2/3}$ 117 dB-$Hz^{4/5}$

Table 1. EA-OEMs at 10 mW optical LO power.

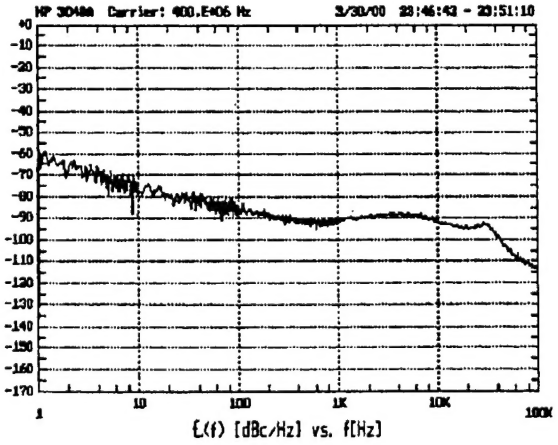

Fig. 4. Absolute phase noise of the RF source driving the MZM (optical LO generator).

Fig. 5. residual phase noise characteristic of the

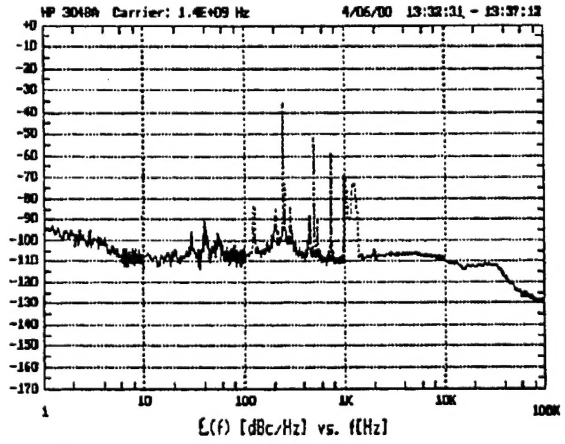

EA-OEM up-converted signal at 1.4 GHz

We have also measured the phase noise characteristics of the converted signals. In the measurement, the optical LO (Fig. 4) is generated via external modulation of a high power laser using a lithium niobate MZM. Fig. 5 shows the residual phase noise spectrum of the up-converted using a 400 MHz optical LO signal.

In conclusion, we have demonstrated that the EA waveguide can be utilized as an OEM that possess low phase noise, large SFDR conversion properties. The conversion loss and SFDR are both dependent on the slope efficiency and saturation power level. At 10-mW LO power, a sub-octave SFDR of 120.0 dB-$Hz^{4/5}$ was achieved with the MQW EA-OEM.

References

1. G. K. Gopalakrishnan, R. P. Moeller, M. M. Howerton, W. K. Burns, K. J. Williams, and R. D. Esman, *IEEE Trans. MTT.*, **43**, pp. 2318-2323, 1995.
2. K.-I. Kitayama, and R. A. Griffin, *IEEE Photon. Technol. Lett.*, **11**, pp. 287-289, 1999.
3. X. S. Yao, and L. Maleki, *IEEE J. Quantum Electron.*, **32**, pp. 1141-1149, 1996.
4. C. K. Sun, R. J. Orazi, and S. A. Pappert, *IEEE Photon. Technol. Lett.*, **8**, pp. 154-156, 1996.
5. R. Helkey, J. C. Twinchell, and C. H. Cox, *J. Lightwave Technol.*, **15**, pp.956-961, 1997.
6. H. Roussell, R. Helkey, *IEEE Microwave Guided Wave Lett.*, **8**, pp. 408-410, 1998.
7. C. P. Liu, A. J. Seeds, and D. Wake, *IEEE Microwave Guided Wave Lett.*, **7**, pp. 72-74, 1997.
8. Y. Betser, D. Ritter, C. P. Liu, A. J. Seeds, and A. Madjar, *J. Lightwave Technol.*, **16**, pp. 605-609, 1998.
9. Y. Betser, J. Lasri, V. Sidorov, S. Cohen, D. Ritter, M. Orenstein, G. Eisensein, A. J. Seeds, and A. Madjar, *IEEE Trans. MTT.*, **47**, pp. 1358-1364, 1999.
10. D. S. Shin, G. L.Li, C. K. Sun, K. K. Loi, W. S. C. Chang, P. K. L. Yu, IEEE Photon. Technol. Lett., **12**, pp. 193-195, 2000.
11. K. K. Loi, J. H. Hodiak, W. B. Mei, C. W. Tu, W. S. C. Chang, D. T. Nichols, L. J. Lembo, and J. C. Brock, *IEEE Photon. Technol. Lett.*, **10**, pp. 1572-1574, 1998.
12. G. L. Li, Y. Z. Liu, R. B. Welstand, C. K. Sun, W. X. Chen, J. T. Zhu, S. A. Pappert, and P. K. L. Yu, *IEEE Photon. Technol. Lett.*, vol. 11, pp.659-61, 1999.